Mon. Not. R. Astron. Soc. **327,** 23–45 (2001)

A multicolour CCD photometric and mass function study of the distant southern open star clusters NGC 3105, NGC 3603, Melotte 105, Hogg 15, NGC 4815, Pismis 20 and NGC 6253

Ram Sagar,[1,2,3★] U. Munari[4★] and K. S. de Boer[3★]

[1]*UP State Observatory, Manora Peak, Naini Tal, 263129, India*
[2]*Indian Institute of Astrophysics, Bangalore, 560034, India*
[3]*Sternwarte der Universität Bonn, Auf dem Hügel 71, D-53121, Bonn, Germany*
[4]*Osservatorio Astronomico di Padova, Sede di Asiago, I-36012 Asiago (VI), Italy*

Accepted 2001 February 19. Received 2001 February 12; in original form 2000 October 31

ABSTRACT

We derive cluster parameters and mass functions from new *UBVRI* CCD photometric observations of ∼3500 stars reaching down to $V \sim 20$ mag for the distant southern open star clusters NGC 3105, NGC 3603, Melotte 105, Hogg 15, NGC 4815, Pismis 20 and NGC 6253. For NGC 3105 and Hogg 15, CCD data are presented for the first time. The reddening is non-uniform across the face of the young (age <300 Myr) clusters NGC 3105, NGC 3603, Melotte 105, Hogg 15 and Pismis 20, with average values of $E(B-V) = 1.06$, 1.44, 0.52, 1.15 and 1.20 mag respectively, while it is uniform with average values of $E(B-V) = 0.72$ and 0.20 mag for the older clusters NGC 4815 and 6253 respectively. The values of colour excess ratios indicate the presence of normal interstellar reddening across the cluster regions studied here. Well-defined main sequences can be seen in all the clusters. However, main-sequence turn-off points and subgiant branches are well defined only in the older clusters NGC 4815 and 6253. The distances to the clusters NGC 3105, NGC 3603, Melotte 105, Hogg 15, NGC 4815, Pismis 20 and NGC 6253 are 9.5 ± 1.5, 7.2 ± 1.2, 2.3 ± 0.2, 3.0 ± 0.3, 2.75 ± 0.2, 3.55 ± 0.35 and 1.8 ± 0.12 kpc respectively, while the corresponding ages derived using theoretical convective core overshooting stellar evolutionary isochrones are 25 ± 10, 3 ± 2, 250 ± 30, 6 ± 2, 400 ± 50, 6 ± 2 and 2500 ± 600 Myr respectively.

In the mass range ∼1–75 $M_\odot$, the mass functions of all clusters except for NGC 6253 have been studied. The slopes of their mass spectra agree within errors with the Salpeter value (1.35). The slope of the mass function for stars more massive than 10 $M_\odot$ is almost the same as for the lower mass stars. The mass function slopes of clusters younger than 500 Myr seem to have no dependence on Galactic longitude, Galactocentric distance and cluster age. As the inherent uncertainties in the mass function determinations of young Galactic star clusters can produce internal scatter that is larger than the external scatter, we conclude that, above 1 $M_\odot$, the initial mass function is universal with a slope of Salpeter value.

Key words: stars: evolution – Hertzsprung–Russell (HR) diagram – stars: luminosity function, mass function – open clusters and associations: general.

1 INTRODUCTION

A study of the luminosity functions (LFs) of 20 star clusters by van den Bergh & Sher (1960) indicates variations in the LFs, with an apparent turnover at fainter magnitudes. Mass functions (MFs) have also been determined recently for a number of open star clusters using homogeneous photoelectric or CCD data and reliable cluster membership (cf. Scalo 1986, 1998; Sagar et al. 1986, 1988; Francic 1989; Sagar & Griffiths 1998b; Kjeldsen & Frandsen 1991; Phelps & Janes 1993; Subramaniam & Sagar 1999). The average MF slope of a young star cluster above 1 $M_\odot$ seems to be not too different from the Salpeter (1955) value derived for the solar neighbourhood, but uncertainties are large and a few objects also showed significant deviations from this average value.

The question of whether the stellar initial mass function (IMF) is

★E-mail: sagar@upso.ernet.in, sagar@iiap.ernet.in (RS); munari@pd.astro.it (UM); deboer@astro.uni-bonn.de (KSdB)

Table 1. Preliminary information about the clusters under study, taken from Lyngå (1987) and Mermilliod (1995).

Cluster designation			Galactic				Trumpler	Radius	distance	$E(B-V)$	age
General	IAU	OCL	l (°)	b (°)	R (kpc)	Z (pc)	class	(arcmin)	(kpc)	(mag)	(Myr)
NGC 3105	C0959−545	798	279.92	0.28	9.6	30	I2p	1.0	8.0	1.09	13
NGC 3603	C1112−609	854	291.62	−0.52	8.2	−46	II3m	2.0	5.3	1.38	10
Melotte 105	C1117−632	856	292.89	−2.45	7.9	−86	I2r	2.0	2.1	0.38	63
Hogg 15	C1240−628	891	302.04	−0.24	7.2	−17	II1p	1.0	4.2	1.16	8
NGC 4815	C1254−646	893	303.63	−2.09	7.6	−102	I2r	2.0	2.8	0.78	200
Pismis 20	C1511−588	932	320.52	−1.21	6.7	−53	I3p	2.2	4.4	1.18	10
NGC 6253	C1655−526	972	335.46	−6.25	7.5	−164	II1m	2.0	1.5	0.23	3000

universal or is instead a function of the environment of star-forming clouds (Larson 1999; Elmegreen 2000) is of fundamental importance not only for understanding the star formation processes but also for evolutionary studies of galaxies. Young star clusters are valuable tools for such studies (cf. Sagar 2000 and references therein). Given the fact that only a few of the large number of Galactic star clusters have been used to study the MF, it is clear that we are at the beginning in utilizing the potential offered by them. In the present work, we derive MF slopes using new CCD photometric observations of the stars in the distant southern open star clusters NGC 3105, NGC 3603, Melotte 105, Hogg 15, NGC 4815, Pismis 20 and NGC 6253, and also in their surrounding fields. Table 1 lists the relevant information available about them, prior to this investigation. Some of these parameters should probably be revised to take account of the new data presented here. The clusters are compact (radius $\leq$2.5 arcmin) and are located at a Galactocentric distance of $\sim$8 kpc in the Galactic disc ($|b| < 7°$). Their ages, values of $E(B-V)$ and heliocentric distances range from $\sim$8 to 3000 Myr, 0.2 to 1.4 mag and 1.5 to 8 kpc respectively. When CCD observations were carried out in 1992, no detailed photometric observations and MF studies in the cluster regions had been published, except for NGC 3603. However, in the meantime some CCD observations have been published for a few of the clusters under study. A brief description of the clusters, along with earlier photometric observations, is given below.

NGC 3105. This is a young distant open cluster which is located in Vela. The first detailed photometric study of the cluster was carried out by Moffat & FitzGerald (1974) in the *UBV* system. They found that the cluster is located at a distance of 8.0 ± 1.5 kpc with reddening $E(B-V) = 1.09 \pm 0.03$ mag. Later on, Fitz-Gerald, Jackson & Moffat (1977) carried out further photoelectric *UBV* observations of 34 stars and confirmed the $E(B-V)$ value but found a smaller distance of 5.5 ± 0.8 kpc. Nevertheless the cluster is a young and distant object, making it a useful spiral arm tracer. It contains a few Be stars.

NGC 3603. This is a luminous, very compact young star cluster which is located at the centre of the most massive visible H II region in the Carina arm of the Galaxy. Its core contains a Trapezium-like system (HD 97950) with about 50 massive stars within a radius of a few arcseconds (Moffat 1983). *Hubble Space Telescope* (*HST*) observations of the cluster region reveal a number of similarities with the core of R136 in 30 Doradus in the Large Magellanic Cloud (Moffat, Drissen & Shara 1994). From photographic photometry, Sher (1965) obtained a distance of 3.5 kpc for this cluster. However, Moffat (1974b) derived a much larger distance of 8.1 ± 0.8 kpc, in agreement with the kinematical distance of 7.2 ± 0.9 kpc (van den Bergh 1978). A distance of 5.3 ± 1.4 kpc to the cluster has been derived by Melnick & Grosbol (1982) using electronographic *UBV* photometry. A CCD *UBV* photometric study by Melnick, Tapia & Terlevich (1989) found a mean value of $E(B-V) = 1.44 \pm 0.13$ mag which is in agreement with the earlier estimate by Moffat (1974b). They derived an average age of $\sim$2 to 3 Myr and showed that star formation is an on-going process in NGC 3603. Based on CCD observations, Pandey, Ogura & Sekiguchi (2000) studied in detail the reddening of the cluster members and found an anomalous reddening law with radial variation in the intracluster material. The stellar content of NGC 3603 has been studied using speckle-masking observations (Hofmann, Seggewiss & Weigelt 1995) and adaptive optics near-infrared imaging from the ground (Eisenhauer et al. 1998).

Melotte 105. This is a compact cluster located about 2° south of the Galactic plane in Carina; it is also known as Collinder 246. Using *UBV* photoelectric and photographic photometry, Sher (1965) derived an age of $\sim$100 Myr, $E(B-V) = 0.38$ mag and a distance of 2.1 kpc. Kjeldsen & Frandsen (1991) carried out a *UBV* CCD photometric study of the cluster and found a distance of 2.2 ± 0.2 kpc, $E(B-V) = 0.52 \pm 0.04$ mag and an age of 150 Myr. Recently, Ahumada et al. (2000) studied the integrated spectral properties of the cluster and derived a low value of $E(B-V) = 0.31 \pm 0.02$ mag and a somewhat younger age of 100 Myr with a metallicity value of 0.0 ± 0.2, in agreement with the earlier determinations by Santos & Bica (1993) using similar observations. However, Balona & Laney (1995) obtained $E(b-y) = 0.32$ mag from *uvby* data, equivalent to $E(B-V) = 0.43$ mag, and a cluster age of 250 Myr. Thus both the reddening and age determinations of the cluster cover a wide range of values.

Hogg 15. This cluster is also known as BH 139 (van den Bergh & Hagen 1975) and ESO95SC15 (Lauberts 1982). It was first recognized as an open cluster by Hogg (1965). An analysis of the photoelectric *UBV* data of 23 stars by Moffat (1974a) yielded $E(B-V) = 1.16$ mag, distance = 4.2 ± 0.4 kpc and age $\sim$8 Myr. Hogg 15 is therefore one of the few clusters known to lie in the second inner arm. The Wolf–Rayet (WR) star HDE 311884 is a probable cluster member. *UBV* and Hβ photoelectric observations of faint early-type stars near the cluster have been carried out by Muzzio, Feinstein & Orsatti (1976). The data suggest large absorption in the direction of the cluster.

NGC 4815. Kjeldsen & Frandsen (1991) have carried out the first CCD *UBV* photometric study of this cluster by measuring 599 stars. They found a distance of 2.8 ± 0.35 kpc, $E(B-V) = 0.78 \pm 0.03$ mag and an age of 200 Myr. Carraro & Ortolani (1994) reported *BV* Johnson CCD photometry of about 2500 stars in the cluster region and derived a distance of 2.5 kpc, $E(B-V) = 0.70$ mag and an age of $\sim$500 Myr. Photometric observations of the cluster have also been carried out by Phelps, Janes & Montgomery

(1994). The spatial distribution and LF of the cluster members have been studied recently by Chen et al. (1998).

Pismis 20. This cluster is regarded as a modest group of young stars located in the association Cir OB1. The distance determination to the open cluster ranges from 2.1 kpc (Moffat & Vogt 1973) to 4.4 kpc (Lyngå 1968). A detailed CCD *UBVR* photometric study of the cluster has been carried out by Vázquez et al. (1995). They found a distance of 3.6 kpc, $E(B-V) = 1.24$ mag and an age of 5 ± 1 Myr. There are a number of WR stars present in the cluster. Turner (1996) has reanalysed the available observations of the cluster and derived a cluster distance of 3.3 ± 0.3 kpc.

NGC 6253. This is an old open cluster located towards the Galactic Centre which is seen projected on a dense field population. After our observations in 1992, both photometric and spectroscopic studies were published for this cluster, indicating the importance of the cluster for the study of Galactic evolution. Bragaglia et al. (1997) presented the first CCD *UBVRI* photometric data, while Piatti et al. (1998) provided CCD *BVI* data and integrated spectra for this cluster. They derived an age of ~3 Gyr, $(m-M)_0 \sim 10.9$ mag, $E(B-V) \sim 0.2$ mag and metallicity significantly higher than the solar value. Based on the integrated spectrum of the cluster, Piatti et al. (1998) obtained a value of [Fe/H] $= +0.2$, while the only high-resolution spectral analysis of four giant stars located in the cluster region yields a value of [Fe/H] $= +0.36 \pm 0.2$ (Carretta et al. 2000). Both spectroscopic and photometric analyses thus indicate a high metallicity value for the cluster members.

The present CCD observations, in combination with earlier observations, have been used to estimate the interstellar extinction to the cluster regions and also to estimate field star contamination, distances and ages of the clusters. The present observations provide the data base for the MF study of these clusters.

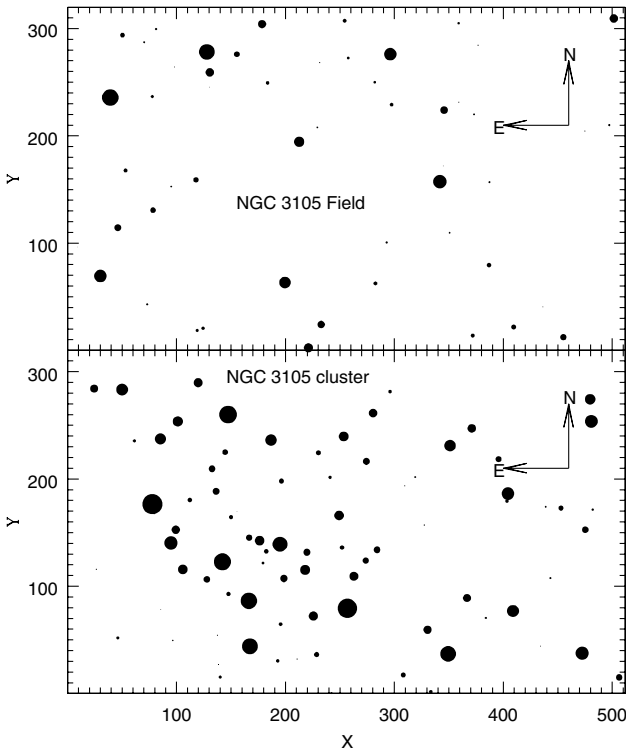

Figure 1. Identification maps for the imaged cluster and field regions of NGC 3105. The (X, Y) coordinates are in pixel units and one pixel corresponds to 0.39 arcsec on the sky. North and east are marked. Filled circles of different sizes represent the brightnesses of the stars. The smallest size denotes stars of $V \sim 18$ mag.

2 OBSERVATIONS

The observations were carried out in 1992 between February 28 and March 8, June 5 and 9, and July 9 and 12 in the Cousins *U*, *B*, *V*, *R* and *I* photometric bands, using an RCA SID53612 thinned CCD detector at the *f*/15.8 Cassegrain focus of the 1.0-m Elizabeth Telescope at the South African Astronomical Observatory (SAAO), Sutherland. At the focus, a 30 μm square pixel of the 320×512 CCD corresponds to 0.39 arcsec and the entire chip covers a field of $\sim 2.1 \times 3.3$ arcmin^2 on the sky. The readout noise for the system was ~73 electron pixel^{-1}, while the number of electrons per ADU was ~11. The photometric quality of the sky was monitored using an off-axis photoelectric photometer that continuously measures a bright, non-variable star located close to the field imaged on the CCD. The nights were of good photometric quality with best and worst seeing ~1.0 and 2.0 arcsec respectively. As the clusters are compact, only one image centred on the object was taken in all the filters. A field region located ~10 to 15 arcmin away from the cluster was also imaged in the *B*, *V* and *I* passbands so that the field star contamination could be derived for the corresponding cluster. Such images were not taken for Hogg 15 and Pismis 20, as strong and patchy variation of interstellar absorption is present around them. Figs 1–7 show the identification maps for the imaged cluster and field regions. Table 2 lists the log of our observations. Only one deep exposure has been taken for the field regions, while generally multiple graded exposures have been obtained for cluster regions. Bias frames were taken intermittently. Prior to each exposure, a 330-ms pre-flash was given to avoid charge transfer problems. Before that the CCD chip was quickly cleaned 50 times and read once. Every hour a 33-s pre-flash was

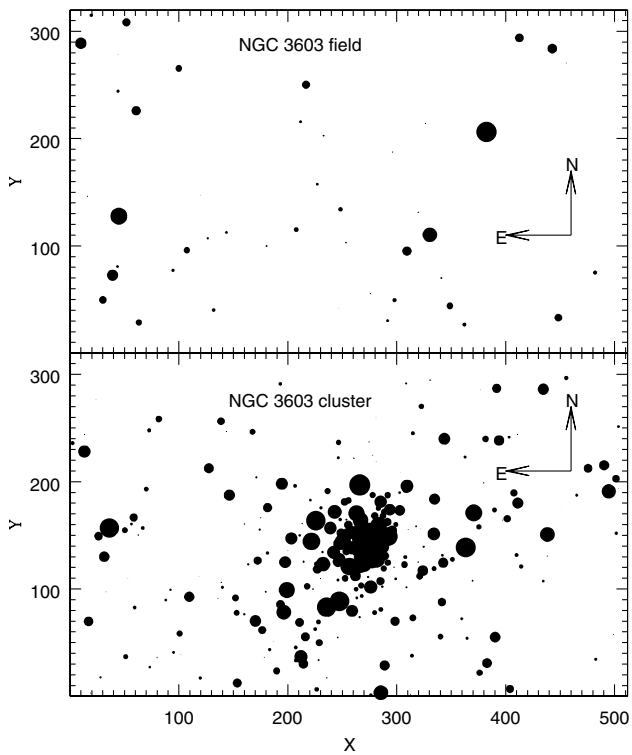

Figure 2. Identification maps for the imaged cluster and field regions of NGC 3603. Other details are the same as in Fig. 1.

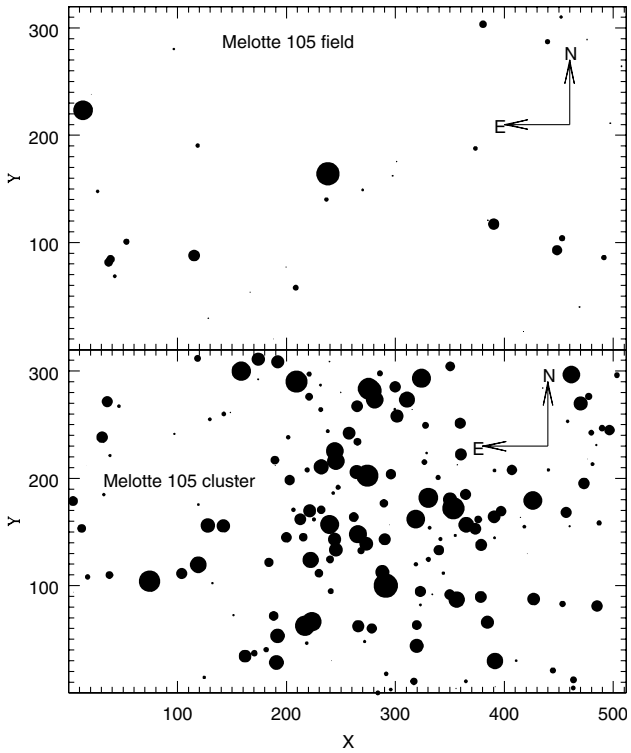

Figure 3. Identification maps for the imaged cluster and field regions of Melotte 105. Other details are the same as in Fig. 1.

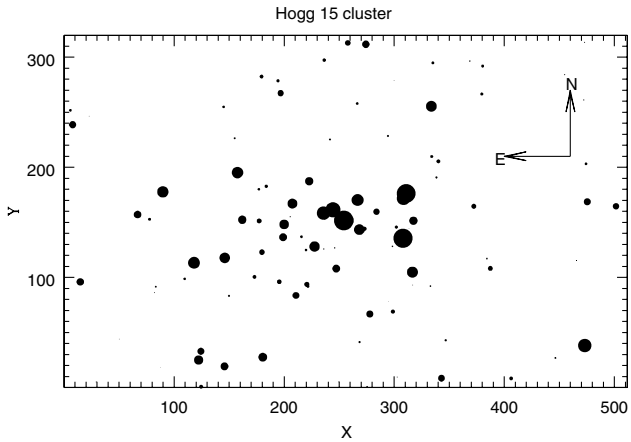

Figure 4. Identification map for the imaged region of the cluster Hogg 15. Other details are the same as in Fig. 1.

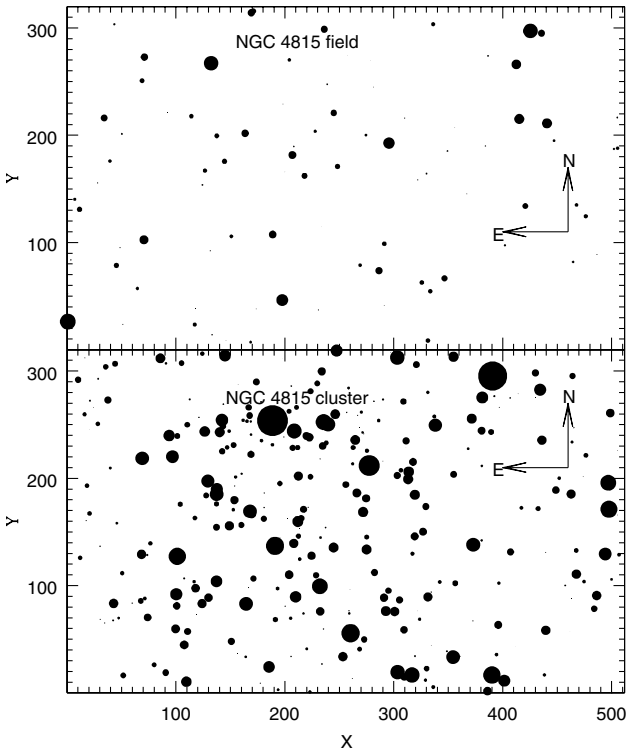

Figure 5. Identification maps for the imaged cluster and field regions of NGC 4815. Other details are the same as in Fig. 1.

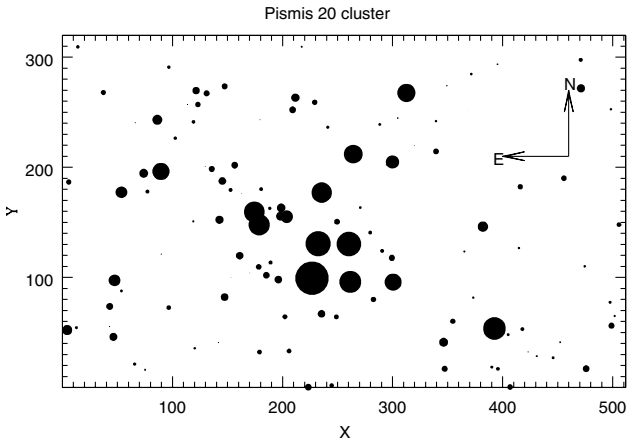

Figure 6. Identification map for the imaged region of the cluster Pismis 20. Other details are the same as in Fig. 1.

acquired to obtain the pre-flash pattern. It was found to be extremely stable with scatter resulting only from photon statistics. Flat-field exposures were made of the twilight sky. Dark current frames were secured in night-time dark conditions.

About 40 E- and F-region standards covering a range in brightness ($7.9 < V < 10.3$) as well as in colour [$0.01 < (V - I) < 2.4$] were observed for calibration purposes. The movement of the CCD camera shutter was monitored by a series of LED–PSD couples that accurately record the *effective* exposure time to 1-ms precision, thus permitting the use of bright photometric standards from the E and F regions. Typically every 1–1.5 h, we observed one red and one blue standard star at small airmass followed by another blue and another red standard star at large airmass in order to have several independent determinations of the primary and secondary extinction coefficients during the night, as well as system colour equations. They were found to be almost constant during an observing run. We used the improved magnitudes of the standard stars provided by the SAAO for calibration purposes. The excellent photometric quality of the sky and the smaller values of airmass at which the observations have been done ensure the accuracy of the data presented here.

3 REDUCTIONS

The data were reduced using the computing facilities available at the SAAO, the Indian Institute of Astrophysics, Bangalore, and the UP State Observatory, Nainital. Initial processing of the data frames was done in the usual manner using the IRAF data reduction package. The flat-field frames were summed for each colour band. The evenness of flat-fields is better than a few per cent in all the filters.

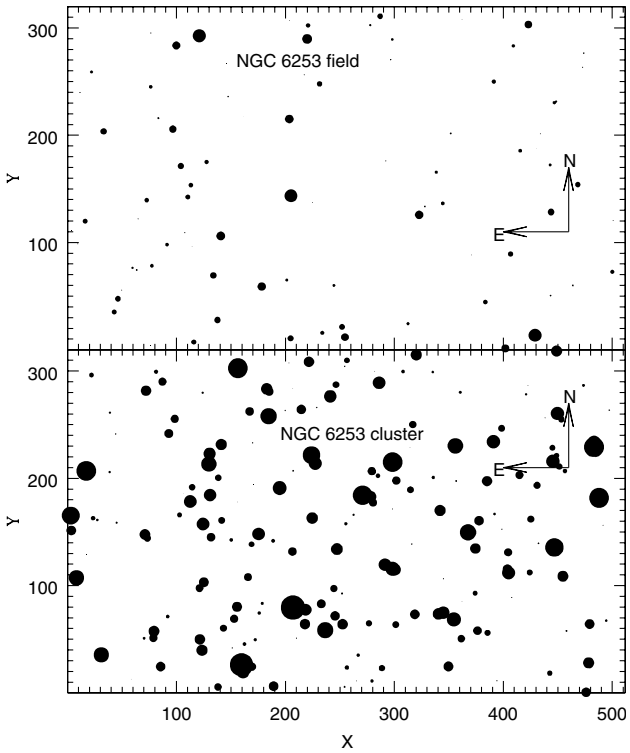

Figure 7. Identification maps for the imaged cluster and field regions of NGC 6253. Other details are the same as in Fig. 1.

Magnitude estimates for stars on the data frames were done using the DAOPHOT software (Stetson 1987, 1992). Further processing and conversion of these raw instrumental magnitudes into the standard photometric system were done using the procedure outlined by Stetson (1992). The image parameters and errors provided by DAOPHOT were used to reject poor measurements. About 10 per cent of the stars were rejected in this process. The DAOMASTER program was used for cross identifying the stars measured on different frames of a cluster region. In those cases where brighter stars are saturated on deep exposure frames, their magnitudes have been taken only from the short exposure frames. Most of the stars brighter than $V \sim 10.5$ mag could not be measured because they are saturated even on the short-exposure frames of the cluster and field regions (see Table 2).

In deriving the colour equations for the CCD system and evaluating the zero-points for the data frames, we have used nightly values of atmospheric extinction coefficients. In the B filter, a mean value (-0.032) for the site is used in the colour term of the atmospheric extinction. The colour equations for the CCD system are determined by performing aperture photometry on the photoelectric standards. By fitting least-squares linear regressions in the observed aperture magnitudes as a function of the standard photometric indices, the following colour equations are derived for the system:

$$\Delta u_{\rm ccd} = \Delta U - 0.02(\pm 0.01)(U - B),$$

$$\Delta b_{\rm ccd} = \Delta B - 0.09(\pm 0.01)(B - V),$$

$$\Delta v_{\rm ccd} = \Delta V + 0.01(\pm 0.007)(B - V),$$

$$\Delta v_{\rm ccd} = \Delta V + 0.02(\pm 0.008)(V - I),$$

$$\Delta r_{\rm ccd} = \Delta R + 0.03(\pm 0.01)(V - R),$$

$$\Delta i_{\rm ccd} = \Delta I + 0.05(\pm 0.01)(V - I),$$

where $UBVR$ and I are the standard magnitudes provided by the SAAO which are the improved values provided by Menzies et al. (1989). $u_{\rm ccd}$, $b_{\rm ccd}$, $v_{\rm ccd}$, $r_{\rm ccd}$ and $i_{\rm ccd}$ are the CCD aperture magnitudes. The colour coefficients agree with those derived independently by Munari & Carraro (1995) and Barbon et al. (2000). To establish the local standards, we selected about 30 isolated stars in each field and used the DAOGROW program for construction of the aperture growth curve required to determine the difference between aperture and profile-fitting magnitudes. These differences, together with the differences in exposure times and atmospheric extinction, were used in evaluating zero-points for local standards in the data frames. The zero-points are uncertain by $\sim$0.02 mag in U and $\sim$0.01 mag in B, V, R and I. The internal errors estimated from the scatter in the individual measures of different exposures in the NGC 6253 cluster region are listed in Table 3 as a function of magnitude for all filters. The errors become large ($>$0.10 mag) for stars fainter than 20 mag. They can be considered as representative of the accuracy of our photometry in all the cluster and field regions under study. The numbers of stars measured in different photometric passbands in a region are given in Table 2. The frequency distribution of stars measured in five passbands is $N(U, B, V, R, I) = (342, 2205, 3480, 1537, 3470)$. The X and Y pixel coordinates as well as the V, $(U - B)$, $(B - V)$, $(V - R)$ and $(V - I)$ magnitudes of the stars observed in the cluster and field regions of NGC 3105, NGC 3603, Melotte 105, Hogg 15, NGC 4815, Pismis 20 and NGC 6253 are listed in Tables 4, 5, 6, 7, 8, 9 and 10 respectively. Only sample tables are presented here; the full tables are available in the electronic version of the article on *Synergy*, on the open star cluster data base web site at http://obswww.unige.ch/webda/, and also with the authors. Wherever possible, we have followed the numbering system adopted by Mermilliod (1995) in the open star cluster data base. Otherwise, stars observed by others have been identified in the last column of each table.

4 COMPARISON WITH PREVIOUS PHOTOMETRY

We compare the present CCD photometry with the available previous photoelectric, electronographic and CCD photometric observations, but not with the photographic data, as they are generally not accurate. For this, we use the open cluster data base prepared by Mermilliod (1995). Sources in the data base are used only when the number of stars in common is at least five. The differences (Δ) in the sense present data minus other data are plotted in Figs 8 to 14 (available in the electronic version of the article on *Synergy*), while the statistical results are given in Table 11. For each cluster of the sample, a brief description of the photometric comparison is given below.

NGC 3105. The present photometry has 23, 12 and 8 stars in common with the photoelectric data given by FitzGerald et al. (1977), Moffat & FitzGerald (1974) and Lyngå & Wramdemark (1973) respectively. The differences (Δ) between the various data sets (see Fig. 8 and Table 11) show that the CCD V magnitudes are systematically fainter than the photoelectric magnitudes, and the difference increases with decreasing brightness and becomes $\sim$0.3 mag for stars fainter than $V \sim 16$ mag. The presence of nebulosity around the cluster appears to be responsible for these differences. Fitting of least-squares linear regressions between Δ and $V, (B - V)$ yields the following relations: $\Delta V = (0.03 \pm 0.02)$ $V - 0.28 \pm 0.28$; $\Delta V = (-0.05 \pm 0.04)(B - V) - 0.27 \pm 0.05$;

Table 2. Log of CCD observations. *N* denotes the number of stars measured in different passbands.

Imaged region	Filter	Exposure (seconds)	Date (1992)	*N*
NGC 3105 cluster	*B*	900	Mar 1	75
	V	85, 600	"	90
	R	600	"	82
	I	60, 600	"	88
NGC 3105 field	*B*	450	Mar 2	40
	V	300	"	70
	I	300	"	70
NGC 3603 cluster	*U*	90, 300	Feb 28	69
	B	40, 120, 900	"	306
	V	20×3, 600	"	431
	R	20×2	"	177
	I	20, 60, 600	"	431
NGC 3603 field	*B*	900	Mar 2	54
	V	300	"	55
	I	600	"	55
Melotte 105 cluster	*U*	300	Mar 2	66
	B	30, 900	"	180
	V	60, 600	"	202
	R	120	"	182
	I	30, 600	"	202
Melotte 105 field	*B*	600	Mar 2	27
	V	400	"	59
	I	400	"	59
Hogg 15 cluster	*U*	600, 900	Mar 6 & 8	42
	B	$120\times2, 900\times2$	"	172
	V	$60, 120\times2, 600\times2$	"	337
	R	$60, 90\times2, 600\times2$	"	327
	I	$30, 60\times2, 600\times2$	"	337
NGC 4815 cluster	*B*	$120\times2, 240, 300\times3, 900\times2$	Jul 9	427
	V	$30\times2, 60, 240\times2, 180, 600\times2$	"	573
	I	$15\times2, 120\times3, 150, 600, 660$	"	573
NGC 4815 field	*B*	900	Jul 11	210
	V	600	"	501
	I	600	"	501
Pismis 20 cluster	*U*	60, 180,240	Jun 5	22
	B	20, 30, 60, 180	"	92
	V	10×2, 12, 60, 180	"	139
	R	2.5×2, 10, 20, 60	"	139
	I	2.5×2, 10, 60	"	139
NGC 6253 cluster	*U*	900×2	Jun 5 & 7	143
	B	$60, 90\times2, 828, 900$	"	436
	V	$30, 60\times3, 600\times2$	"	682
	R	$18, 2060, 90, 600\times2$	"	630
	I	$5, 15, 60, 600\times2$	"	674
NGC 6253 field	*B*	900	Jun 8	186
	V	600	"	341
	I	600	"	341

Table 3. Internal photometric errors in magnitudes as a function of brightness in the NGC 6253 cluster region. σ is the standard deviation per observation in magnitudes.

Magnitude range	σ_U	σ_B	σ_V	σ_R	σ_I
≤14.0	0.002	0.001	0.003	0.012	0.02
14.0–15.0	0.01	0.005	0.02	0.03	0.04
15.0–16.0	0.01	0.01	0.02	0.03	0.04
16.0–17.0	0.03	0.02	0.03	0.04	0.04
17.0–18.0	0.06	0.04	0.04	0.05	0.05
18.0–19.0	0.08	0.05	0.05	0.07	0.07
19.0–20.0	0.09	0.07	0.08	0.08	0.08

$\Delta(B-V) = (-0.03 \pm 0.01)\quad V + 0.43 \pm 0.17$; $\Delta(B-V) = (0.04 \pm 0.02)\,(B-V) - 0.01 \pm 0.03$. The correlation coefficients of all these linear relations are ∼0.3.

NGC 3603. The photoelectric data provided by Moffat (1974b) and van den Bergh (1978) have 10 and 11 stars respectively in common with present photometry, while the electronographic data of Melnick & Grosbol (1982) and the CCD data of Melnick et al. (1989) have 12 and 131 stars respectively common. The differences of these data (see Fig. 9 and Table 11) show that they agree fairly well with the present photometry, except for the photoelectric data by Moffat (1974b).

Melotte 105. The present CCD photometry has 108 stars in common with the CCD data of Kjeldsen & Frandsen (1991). The plot of the differences between the two data sets in Fig. 10 and their statistical results in Table 11 indicate good agreement between them.

Hogg 15. There are 19 stars in common between the present CCD and Moffat (1974a) photoelectric data. The differences between them are plotted in Fig. 11 and the statistical results are listed in Table 11. They show that in general the *UBV* photoelectric

Table 4. CCD relative positions and photometric magnitudes of a few stars, as a sample, measured in the NGC 3105 cluster and field regions. The entire data set is available in electronic form (see text). In the cluster region, stars observed earlier have the numbering system of Moffat & FitzGerald (1974) taken from the cluster data base, while the numbering of stars observed for the first time by us starts with 201 in column 1. In the field region, stars observed by us are numbered in increasing order of X value.

Star	X (pixel)	Y (pixel)	V (mag)	$(B-V)$ (mag)	$(V-R)$ (mag)	$(V-I)$ (mag)
			NGC 3105 cluster region			
1	77.76	176.49	12.48	1.00	0.76	1.27
3	99.31	152.69	15.71	1.15		0.91
4	94.85	140.35	14.34	0.94	0.76	1.19
5	105.76	115.72	15.30	0.93	0.57	0.99
6	127.87	106.42	16.17	1.03	0.61	0.85
			NGC 3105 field region			
1	8.99	96.34	17.87	1.05		1.34
2	30.06	69.37	14.56	0.89		1.18
3	33.55	236.90	16.89			1.09
4	39.15	235.75	13.47	0.78		1.08
5	46.05	114.47	16.08	0.95		1.12

data are in good agreement with the present CCD data. For four stars, in comparison with photoelectric values, CCD V magnitudes are fainter by more than 0.3 mag, but the CCD $(B-V)$ and $(U-B)$ colours agree fairly well with their corresponding photoelectric values. Inspection of CCD images indicates that photoelectric measurements of these stars have been affected by the presence of one or more nearby stars of similar colours but $\geq$0.5 mag fainter in V. The agreement between the photoelectric and present CCD data becomes excellent if the total light of the star and its companion(s) in the CCD measurement is calculated, mimicking aperture photometry.

NGC 4815. There are nine stars in common between the photoelectric photometry of Moffat & Vogt (1973) and the present CCD measurements. There are 229 stars from Kjeldsen & Frandsen (1991), 459 stars from Carraro & Ortolani (1994) and 409 stars from Phelps et al.'s (1994) CCD data with positions that coincide within 1 pixel with the stars measured by us. The differences (Δ) between the present data and the data obtained by others (see Fig. 12 and Table 11) show that except for the V values of Phelps et al. (1994) and a few outliers, which appear to be

Table 5. CCD relative positions and magnitudes of a few stars, as a sample, measured in the NGC 3603 cluster and field regions. The entire data set is available in electronic form (see text). In the cluster region, stars observed earlier have the numbering system of Sher (1965) taken from the cluster data base, while the numbering of stars observed for the first time by us starts with 301 in column 1. In the field region, stars observed by us are numbered in increasing order of X value.

Star	X (pixel)	Y (pixel)	V (mag)	$(U-B)$ (mag)	$(B-V)$ (mag)	$(V-R)$ (mag)	$(V-I)$ (mag)
				NGC 3603 cluster region			
4	13.19	228.12	14.61		1.65	1.12	2.40
5	36.09	156.92	12.65	−0.08	0.69	0.55	1.07
17	494.62	191.03	14.09	−0.01	1.21	0.98	1.85
18	247.34	88.55	12.62	−0.03	1.21	0.96	1.83
19	199.13	99.07	13.56	−0.14	1.03	0.78	1.49
				NGC 3603 field region			
1	9.94	288.85	14.85		1.63		1.90
2	10.03	198.77	17.81		0.86		1.39
3	15.53	146.37	18.00		1.08		1.21
4	19.56	314.99	17.06		0.98		1.22
5	30.17	49.69	15.88		0.76		1.06

Table 6. CCD relative positions and magnitudes of a few stars, as a sample, measured in the Melotte 105 cluster and field regions. The entire data set is available in electronic form (see text). In the cluster region, stars observed earlier have the numbering system of Sher (1965) taken from the cluster data base, while the numbering of stars observed for the first time by us starts with 501 in column 1. In the field region, stars observed by us are numbered in increasing order of X value.

Star	X (pixel)	Y (pixel)	V (mag)	$(U-B)$ (mag)	$(B-V)$ (mag)	$(V-R)$ (mag)	$(V-I)$ (mag)
				Melotte 105 cluster region			
4	158.37	299.85	12.68	0.12	0.50	0.20	0.59
5	209.16	290.14	11.92	0.22	0.51	0.21	0.62
6	264.83	267.28	14.79	0.42	0.56	0.29	0.74
7	323.93	293.27	12.77	0.22	0.51	0.21	0.61
8	426.15	179.29	12.84	0.18	0.45	0.18	0.57
				Melotte 105 field region			
1	13.12	223.36	12.58		0.48		0.56
2	20.13	225.17	16.94				1.18
3	20.84	238.12	17.80		1.11		3.00
4	22.89	275.94	18.25				3.48
5	26.58	147.68	17.01		1.74		2.12

Table 7. Relative positions and CCD *UBVRI* magnitudes of a few stars, as a sample, measured in the field of Hogg 15. The entire data set is available in electronic form (see text). Stars observed by Moffat (1974b) and Feinstein & Marraco (1971) have been prefixed with M and FM respectively in the last column.

Star	X (pixel)	Y (pixel)	V (mag)	$(U-B)$ (mag)	$(B-V)$ (mag)	$(V-R)$ (mag)	$(V-I)$ (mag)	Other identifications
1	−0.49	38.54	16.22			0.76	1.63	
2	4.23	180.78	17.84		1.25	0.70	1.51	
3	5.76	251.77	17.18		1.09	0.71	1.50	
4	7.76	238.73	15.86	0.24	0.86	0.55	1.12	
232	310.89	176.29	12.40	−0.19	0.89	0.57	1.14	M2, FM2

Table 8. CCD relative positions and magnitudes of a few stars, as a sample, measured in the NGC 4815 cluster and field regions. The entire data set is available in electronic form (see text). In the cluster region, numbering system of stars observed earlier is taken from the cluster data base, while the numbering of stars observed for the first time by us starts with 9001 in column 1. In the field region, stars observed by us are numbered in increasing order of X value.

Star	X (pixel)	Y (pixel)	V (mag)	$(B-V)$ (mag)	$(V-I)$ (mag)
NGC 4815 cluster region					
3429	560.28	23.99	15.62	0.93	0.43
3443	558.81	236.16	17.28	0.93	0.53
9001	13.46	127.97	18.28		1.67
9002	35.85	312.28	19.54		2.38
9003	65.12	132.08	18.28	0.49	1.14
NGC 4815 field region					
1	0.42	52.13	17.57	1.41	1.53
2	0.73	26.22	13.65	1.38	1.40
3	2.32	101.88	19.81		2.12
4	3.13	259.69	19.96		1.91
5	3.47	83.78	17.61		1.61

mostly stars that were treated as single in one study and as blended doubles in other studies, the distribution of the photometric differences seems fairly random with a constant zero-point offset. As expected, the scatter increases with decreasing brightness and becomes more than ∼0.1 mag at fainter levels.

Pismis 20. A comparison of the present CCD photometry with photoelectric data given by Muzzio (1979), Moffat & Vogt (1973), Lyngå (1968) and Peterson & FitzGerald (1988) and with CCD data reported by Vázquez et al. (1995) is shown in Fig. 13, and statistical results are listed in Table 11. Our V magnitudes are systematically brighter by ∼0.03 mag than photoelectric values. However, they are about 0.1 mag brighter than the CCD V values given by Vázquez et al. (1995). Both photoelectric and CCD colours of earlier observations agree very well with the present CCD photometric colours.

NGC 6253. Our CCD photometric data have 550 and 122 stars in common with those of Bragaglia et al. (1997) and Piatti et al. (1998) respectively. The variations of photometric differences between these data sets are plotted as a function of brightness in Fig. 14, and statistical results are given in Table 11. They show that, except for a few outliers, which appear to be mostly stars that were treated as single in one study and as blended doubles in other studies, the distribution of photometric differences seems fairly random with a constant zero-point offset. As expected, the scatter increases with decreasing brightness. The present photometry is ∼0.1 mag brighter in V, redder in $(U-B)$ and bluer in $(V-I)$ in comparison with earlier photometry. However, the $(B-V)$ and $(V-R)$ colours agree fairly well.

Barbon et al. (2000), Munari, Carraro & Barbon (1998), Munari & Carraro (1996) and Munari & Carraro (1995) have shown that SAAO CCD photometry is generally in excellent agreement with other published accurate CCD photometries, while the photoelectric data in crowded cluster regions are systematically off in the sense of being too bright, and for the bluest stars too red, exactly what one would expect from fainter red stars entering the diaphragm of the photoelectric measurement. The present study confirms this, as the agreement is good between profile photometries and poor against aperture photometries. Keeping this in mind, we now turn to deriving cluster parameters by combining the present data with the published data wherever necessary.

5 RADIAL STELLAR SURFACE DENSITY AND FIELD STAR CONTAMINATION

The radial variation of stellar surface density derived from the present data can be used to verify clustering and also to estimate the extent of field star contamination in the cluster region. For this,

Table 9. CCD relative positions and magnitudes of a few stars, as a sample, measured in the field of Pismis 20. The entire data set is available in electronic form (see text). Stars observed earlier have numbering system of Vázquez et al. (1995), while the numbering of stars observed for the first time by us starts with 501 in column 1.

Star	X (pixel)	Y (pixel)	V (mag)	$(U-B)$ (mag)	$(B-V)$ (mag)	$(V-R)$ (mag)	$(V-I)$ (mag)
37	13.99	309.35	16.95			0.26	1.44
39	117.56	307.66	18.28			0.79	1.63
42	470.95	297.57	16.78			0.78	1.64
501	12.71	54.39	17.08		1.31	0.83	1.67
502	42.55	194.21	18.22			1.04	1.95

Table 10. CCD relative positions and magnitudes of a few stars, as a sample, measured in the NGC 6253 cluster and field regions. The entire data set is available in electronic form (see text). In the cluster region, stars observed earlier have the numbering system of Bragaglia et al. (1997) taken from the cluster data base, while the numbering of stars observed for the first time by us starts with 6001 in column 1. In the field region, stars observed by us are numbered in increasing order of X value.

Star	X (pixel)	Y (pixel)	V (mag)	$(U-B)$ (mag)	$(B-V)$ (mag)	$(V-R)$ (mag)	$(V-I)$ (mag)
			NGC 6253 cluster region				
1300	476.00	0.53	15.38	0.43	0.86	0.50	0.93
1309	313.40	−1.06	16.29		1.37	0.18	0.64
6001	1.22	296.57	20.18			0.58	1.38
6002	2.58	262.06	19.69			0.70	1.27
6003	3.45	123.86	20.99			0.19	1.34
			NGC 6253 field region				
1	2.10	158.87	18.58		1.05		1.06
2	3.51	46.98	18.86		1.05		0.89
3	3.80	111.37	17.85		1.00		0.99
4	4.75	309.49	18.23				0.93
5	8.98	298.69	19.52				1.02

the cluster centre is first fixed. We have derived it iteratively by calculating average X and Y positions of stars within 150 pixels from an eye-estimated centre, until it converged to a constant value (see Table 12). An error of about 10 to 20 pixels is expected in locating the cluster centre. For NGC 6253, the presented cluster centre is not too different from the eye estimate by Bragaglia et al. (1997). To determine the radial surface density of stars in a cluster, the imaged area has been divided into a number of concentric circles with respect to the above-estimated cluster centre, in such a way that each zone contains at least 10 stars. The number density of stars, ρ_i, in the ith zone has been evaluated as

$$\rho_i = \frac{N_i}{A_i},$$

where N_i is the number of stars and A_i is the area of the ith zone. The stellar surface densities derived in this way are shown in Fig. 15 in the form of $\log \rho$ versus radius (R) plots. The stellar surface density is highest for NGC 6253 and lowest for NGC 3105. However, the presence of clear radius–density variations confirms a relatively small diameter and the existence of clustering in the objects under study, except for NGC 6253. For this cluster, the radial variation of stellar density has also been compared with that derived using the data for a larger (7×7 arcmin^2) area from Bragaglia et al. (1997). Both radial density profiles agree fairly well. The lack of a clear decline in stellar density profile with radius may indicate that the true cluster radius is larger than that given in Table 1, as has also been indicated by Bragaglia et al. (1997).

The level of field star density derived from the imaged region is also shown in Fig. 15. For all clusters, except NGC 4815, the field star level is lower than the last outer points of the cluster radial stellar density profile (see Fig. 15). This indicates that the imaged areas of the cluster regions are not large enough for the determination of cluster radius. It can be seen that the extent of field star contamination is similar in NGC 3105, NGC 3603 and Melotte 105, but significantly smaller than that in NGC 4815 and NGC 6253. The field star densities up to $V = 18$ mag are ∼7.6, 6.9, 5.3, 12.6 and 9.9 arcmin^{-2} for NGC 3105, NGC 3603, Melotte 105, NGC 4815 and NGC 6253 respectively. However, they increase drastically below $V = 18$ mag. From these numbers, as well as the cluster sequences present in the colour–magnitude diagrams discussed later, one may say that, except for NGC 4815 and NGC 6253, the field star contamination in the stars brighter than $V \sim 18$ mag is not strong enough to smear the cluster sequences and hence affect the results derived below.

In order to see whether the radial stellar surface density distribution within a cluster radius follow $\rho \propto e^{-BR}$ or $\rho \propto R^{-\gamma}$, we fitted the linear relations $\ln \rho(R) = \text{constant} - BR$ and $\log \rho(R) = \text{constant} - \gamma \log R$ between ρ and R using least-squares solutions. The values of B and γ with their standard deviations σ_B and σ_γ are given in Table 12. Except for NGC 6253, the values of the correlation coefficients $|r|$ for both the relations are similar and also equal to 1.0. The radial stellar surface density distribution within a cluster radius can therefore be represented equally well by both relations. Poor fitting of both relations in the case of NGC 6253 may be a result of lack of clustering in the object. A comparison of these with the corresponding values derived for the clusters NGC 6603, NGC 7044, Berkeley 81 and Berkeley 99 by Sagar & Griffiths (1998a) indicates that in the objects where clustering is present, the B values range from 0.003 to 0.008, while the γ values range from 0.2 to 0.8. However, a larger sample of star clusters is required to understand the cause of variation in the values of B and γ.

6 APPARENT COLOUR–MAGNITUDE DIAGRAMS OF CLUSTER AND FIELD REGIONS

The apparent colour–magnitude (CM) diagrams generated from the present data for the clusters NGC 3105, NGC 3603, Melotte 105 and NGC 4815 and their field regions if observed are displayed in Fig. 16, while the corresponding diagrams for Hogg 15, Pismis 20 and NGC 6253 are shown in Fig. 17. The $V, (V-I)$ diagram of a cluster is the deepest one, and generally extends down to $V = 20$ mag. A well-defined cluster main sequence (MS) contaminated by field stars is clearly visible in all CM diagrams. The extent of field star contamination seems to vary from cluster to cluster as expected. It is more important for NGC 4815 and NGC 6253. The cluster sequences fainter than $V = 18$ mag have large scatter and are perhaps not clearly defined. This may be due to photometric errors as well as field star contamination. It is difficult to separate field stars from the cluster members only on the basis of

Table 11. Statistical results of the photometric comparison. The magnitude difference (Δ) is always in the sense present minus comparison data. The mean and standard deviation (σ) are based on N stars. A few points discrepant by more than 3.5σ have been excluded from the analysis. Photoelectric, electronographic and CCD observations have been abbreviated as pe, el and CCD respectively, and always written inside the bracket with the abbreviated author names.

Comparison data	V range (mag)	ΔV Mean $\pm\sigma$	N	$\Delta(B-V)$ Mean $\pm\sigma$	N	$\Delta(U-B)$ Mean $\pm\sigma$	N	$\Delta(V-R)$ Mean $\pm\sigma$	N	$\Delta(V-I)$ Mean $\pm\sigma$	N
NGC 3105: comparison data are from Lyngå & Wramdemark (1973)(LW), Moffat & FitzGerald (1974)(MF) and Fitzgerald et al. (1977)(F)											
LW(pe)	12.0–16.0	0.21 ± 0.13	8	0.08 ± 0.07	8						
MF(pe)	12.0–16.0	0.23 ± 0.16	12	0.06 ± 0.03	12						
F(pe)	12.0–17.0	0.19 ± 0.18	23	0.03 ± 0.12	23						
NGC 3603: comparison data are from Melnick et al. (1989)(MTT), Melnick & Grosbol (1982)(MG), Moffat (1974b)(M) and van den Bergh (1978)(V)											
M(pe)	12–15	0.13 ± 0.21	10	0.06 ± 0.06	10	0.13 ± 0.08	10				
V(pe)	12–15	-0.07 ± 0.08	11	0.01 ± 0.05	11	-0.02 ± 0.07	11				
MG(el)	13–15	-0.03 ± 0.13	12	0.03 ± 0.06	12	-0.03 ± 0.27	12				
MTT(CCD)	12–14	-0.02 ± 0.12	21	0.03 ± 0.12	21	0.13 ± 0.13	20				
	14–16	-0.04 ± 0.06	60	0.02 ± 0.04	60	0.12 ± 0.09	31				
	16–18	-0.02 ± 0.12	38	0.03 ± 0.10	37						
Melotte 105: comparison data are from Kjeldsen & Frandsen (1991)(KF)											
KF(CCD)	11–17	-0.02 ± 0.06	102	0.02 ± 0.06	97	0.00 ± 0.18	52				
Hogg 15: comparison data are from Moffat (1974a)(M)											
M(pe)	12–15	-0.06 ± 0.08	14	0.03 ± 0.05	17	0.02 ± 0.11	16				
NGC 4815: comparison data are from Moffat & Vogt (1973)(MV), Kjeldsen & Frandsen (1991)(KF), Carraro & Ortolani (1994)(CO) and Phelps et al. (1994)(PJ)											
MV(pe)	9–14	-0.06 ± 0.11	7	0.01 ± 0.08	9						
KF(CCD)	11–17	-0.03 ± 0.11	212	-0.01 ± 0.08	193						
CO(CCD)	11–19	0.03 ± 0.12	427	-0.02 ± 0.11	355						
PJ(CCD)	11–18	0.25 ± 0.15	387							-0.02 ± 0.19	398
Pismis 20: comparison data are from Muzzio (1979)(MU), Moffat & Vogt (1973)(MV), Peterson & FitzGerald (1988)(PF), Lyngå (1968)(L) and Vázquez et al. (1995)(V)											
MU(pe)		-0.04 ± 0.01	2	0.01 ± 0.01	2	-0.04 ± 0.02	2				
MV(pe)	9–14	-0.02 ± 0.06	9	0.04 ± 0.05	9	-0.04 ± 0.03	10				
PF(pe)	9–14	-0.02 ± 0.08	10	0.00 ± 0.05	10	-0.02 ± 0.02	10				
L(pe)	9–14	-0.03 ± 0.03	12	0.02 ± 0.01	10	0.06 ± 0.06	12				
V(CCD)	10–19	-0.10 ± 0.04	83	0.01 ± 0.06	61	-0.04 ± 0.04	18	-0.06 ± 0.05	83		
NGC 6253: comparison data are from Bragaglia et al. (1997)(B) and Piatti et al. (1998)(P)											
B(CCD)	11–21	-0.13 ± 0.10	437	-0.01 ± 0.09	350	0.08 ± 0.14	141	0.00 ± 0.09	495	-0.09 ± 0.11	499
P(CCD)	11–18	-0.07 ± 0.05	115	-0.02 ± 0.07	117					-0.14 ± 0.06	113

Table 12. Exponential powers of the variation of stellar surface density (ρ) with radius (R) in the relations $\rho\propto e^{-BR}$ and $\rho\propto R^{-\gamma}$. r_1 and r_2 are correlation coefficients of least-square solutions of the linear relations used to derive the values of B and γ respectively. The (X_c,Y_c) values denote pixel coordinates of the cluster centre.

Cluster	X_c	Y_c	$B\pm\sigma_B$	$\lvert r_1\rvert$	$\gamma\pm\sigma_\gamma$	$\lvert r_2\rvert$
NGC 3105	180	140	0.007 ± 0.001	0.95	0.51 ± 0.05	0.98
NGC 3603	250	140	0.007 ± 0.002	0.90	0.75 ± 0.08	0.97
Melotte 105	285	175	0.005 ± 0.001	0.88	0.38 ± 0.17	0.75
Hogg 15	200	140	0.006 ± 0.001	0.98	0.47 ± 0.06	0.97
NGC 4815	210	185	0.004 ± 0.001	0.98	0.32 ± 0.08	0.91
Pismis 20	170	160	0.008 ± 0.002	0.88	0.59 ± 0.13	0.93
NGC 6253	270	180	0.001 ± 0.001	0.30	0.08 ± 0.08	0.46

their closeness to the main populated area of the CM diagrams, because field stars at cluster distance and reddening also occupy this area (see Figs 16 and 17). The exception is NGC 3603 where the bulk of the field population seems to lie in front of the heavily reddened cluster and thus appears to be clearly separated from field stars. For the separation of cluster members from the field stars, precise proper motion and/or radial velocity measurements of these stars are required. In the absence of such data, we used photometric criteria for cluster membership. A star is considered as a probable cluster member if it lies close to the cluster sequence at least in one of the apparent CM diagrams of the cluster region. The frequency distribution of such probable members shows that the fraction of photometric non-members lies in the range of 14–28 per cent, being lowest in Hogg 15 and largest in NGC 3603. From the $V,(V-I)$ diagram of the field region of a cluster, the statistically

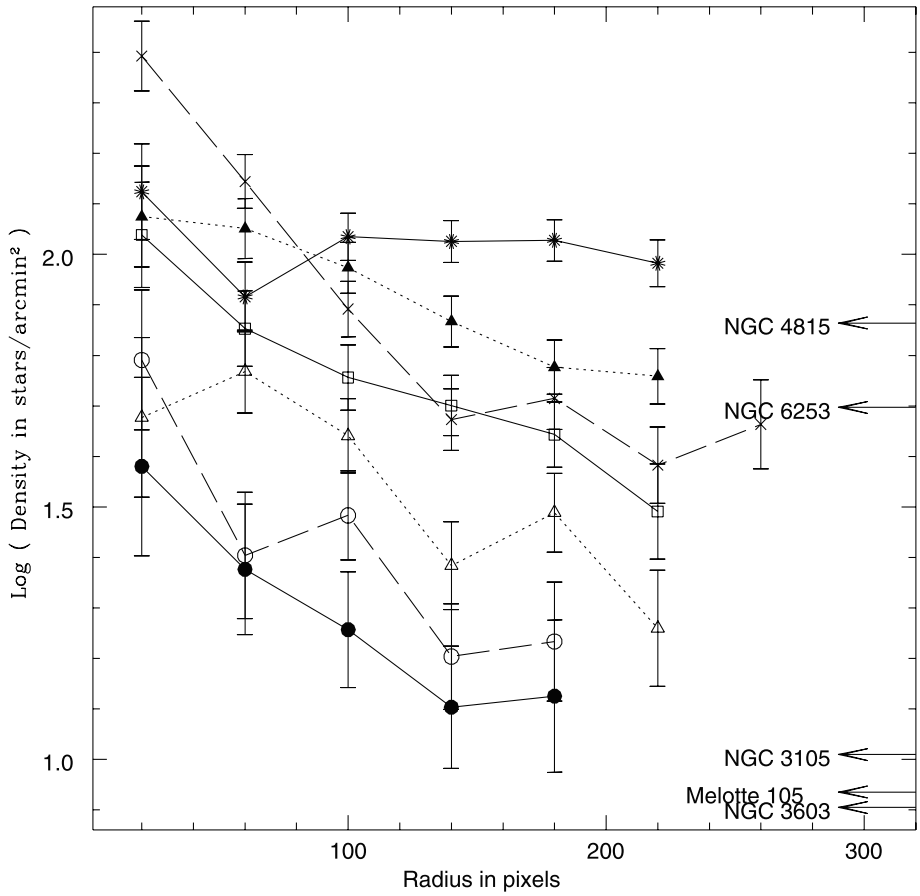

Figure 15. The variation of stellar surface density with radius for NGC 3105 (filled circles), NGC 3603 (crosses), Melotte 105 (open triangles), Hogg 15 (open squares), NGC 4815 (filled triangles), Pismis 20 (open circles) and NGC 6253 (asterisks). The length of the bar represents errors resulting from sampling statistics ($= 1/N^{1/2}$, where N is the number of stars used in the density estimate at that point). Horizontal arrows show the level of field star contamination estimated from the regions imaged by us. The values are 10.2, 8.0, 8.6, 73.1 and 49.8 star arcmin^{-2} for the field regions of NGC 3105, NGC 3603, Melotte 105, NGC 4815 and NGC 6253 respectively.

expected number of field stars among the photometric cluster members has also been determined and is given in Table 13. It is thus clear that all photometric probable members cannot be cluster members, and non-members should be subtracted in the studies of cluster MF, etc. However, they can be used to determine the cluster parameters, and this has been done in the sections to follow.

The morphological features present in the apparent CM diagrams (Figs 16 and 17) indicate that NGC 3105, NGC 3603, Hogg 15 and Pismis 20 are young ($<$100 Myr), as stellar evolutionary signatures are barely visible amidst the brighter cluster members. On the other hand, the presence of a well defined MS turn-off point along with giant stars in the case of Melotte 105, NGC 4815 and NGC 6253 indicates that they are relatively older clusters. As the procedures for parameter determination are different for young and old star clusters, we used the procedure suitable for the particular cluster age.

7 INTERSTELLAR EXTINCTION IN THE DIRECTION OF YOUNG CLUSTERS

It is well known that the apparent $(U-B)$ versus $(B-V)$ diagrams of young clusters containing A0 or earlier spectral type stars are very useful for estimating interstellar extinction to the clusters. We therefore plot, in Fig. 18, such diagrams for the young clusters NGC 3603, Melotte 105, Hogg 15 and Pismis 20 where U measurements were carried out by us. To separate the early-type MS stars in these clusters, we have also used the corresponding apparent $V,(U-V),V,(B-V),V,(V-R)$ and $V,(V-I)$ diagrams shown in Figs 16 and 17. Adopting the slope of the reddening line $E(U-B)/E(B-V)$ as 0.72, we fit in Fig. 18 the intrinsic zero-age main sequence (ZAMS) given by Schmidt-Kaler (1982) to the MS stars of spectral type earlier than A0. This indicates that all young clusters have differential reddening across the cluster face with $E(B-V)$ values in magnitudes ranging from about 1.1 to 1.6 for NGC 3603, 0.45 to 0.78 for Melotte 105, 1.05 to 1.25 for Hogg 15 and 1.15 to 1.37 for Pismis 20. For NGC 3105, $E(B-V)$ has been estimated using the present $(B-V)$ data and the $(U-B)$ data from FitzGerald et al. (1977), and found to vary from 0.94 to 1.22.

As the factors other than non-uniform (differential) extinction such as peculiarities, binaries etc., along with photometric errors, can produce a maximum dispersion in $E(B-V)$ of $\sim$0.11 mag for MS members (see Sagar 1987 for a detailed discussion), we considered the presence of variable extinction in the cluster region, if the difference between the maximum and minimum $E(B-V)$ values for MS members is more than 0.11 mag. The observed large values of this difference indicate that interstellar extinction is not uniform across the face of the clusters NGC 3105, NGC 3603, Melotte 105, Hogg 15 and Pismis 20. This may be due to the presence of varying amounts of matter either inside the cluster or in

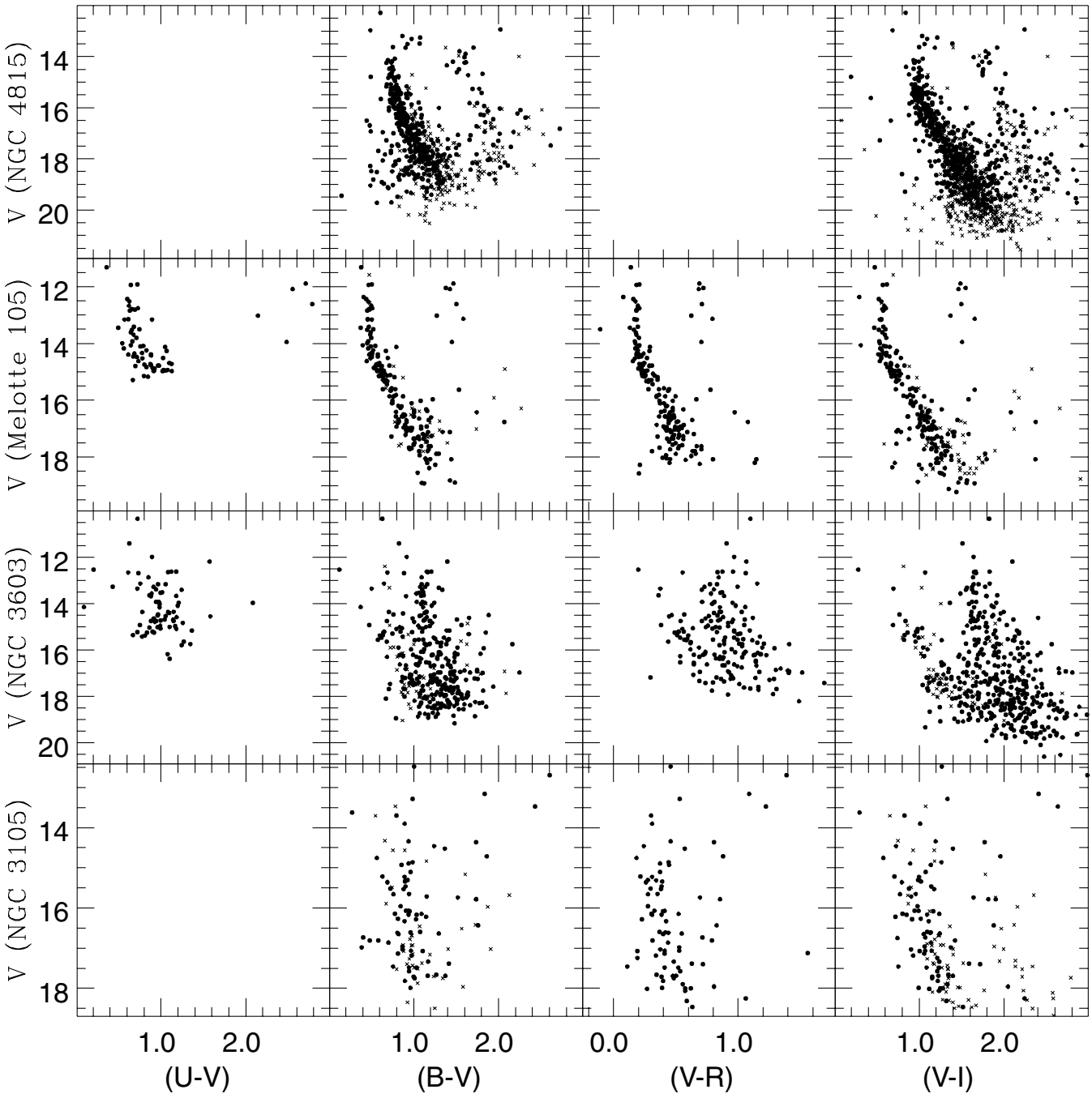

Figure 16. The $V, (U-V), V, (B-V), V, (V-R)$ and $V, (V-I)$ diagrams for the stars observed by us in the cluster (filled circles) and field (crosses) regions of NGC 3105, NGC 3603, Melotte 105 and NGC 4815.

its foreground interstellar medium. In NGC 3603, Pandey et al. (2000) have also found radial variation of the reddening with a minimum near the cluster centre.

To determine the nature of the interstellar extinction law in the direction of these young clusters, we used stars having spectral type earlier than A0. This has been judged from their locations in the $(U-B)$ versus $(B-V)$ and apparent CM diagrams, which reveal that bright stars with $V < 16$ mag and $(B-V) < 1.5$ mag in NGC 3105; with $V < 14$ and $(B-V) < 1.0$ mag in Melotte 105 and with $V < 15.5$ and $(B-V) < 1.3$ mag in both Hogg 15 and Pismis 20 are the desired objects. There are 15, 23, 19 and 20 such stars in NGC 3105, Melotte 105, Hogg 15 and Pismis 20 respectively. In the case of NGC 3603, data available in the literature have also been used. Drissen et al. (1995) have provided spectral classification for 14 stars in the central core of NGC 3603 using *HST* observations. For these stars B magnitudes are taken from the *HST* photometric measurements of Moffat et al. (1994). In addition to these, there are 11 stars for which spectral classifications are available from the open cluster data base. The near-infrared adaptive optics imaging of the NGC 3603 core by Eisenhauer et al. (1998) provides the *JHK* magnitudes of the stars. Spectroscopy and near-infrared photometry have been used along with the available *UBVRI* observations to study the interstellar extinction in the cluster NGC 3603.

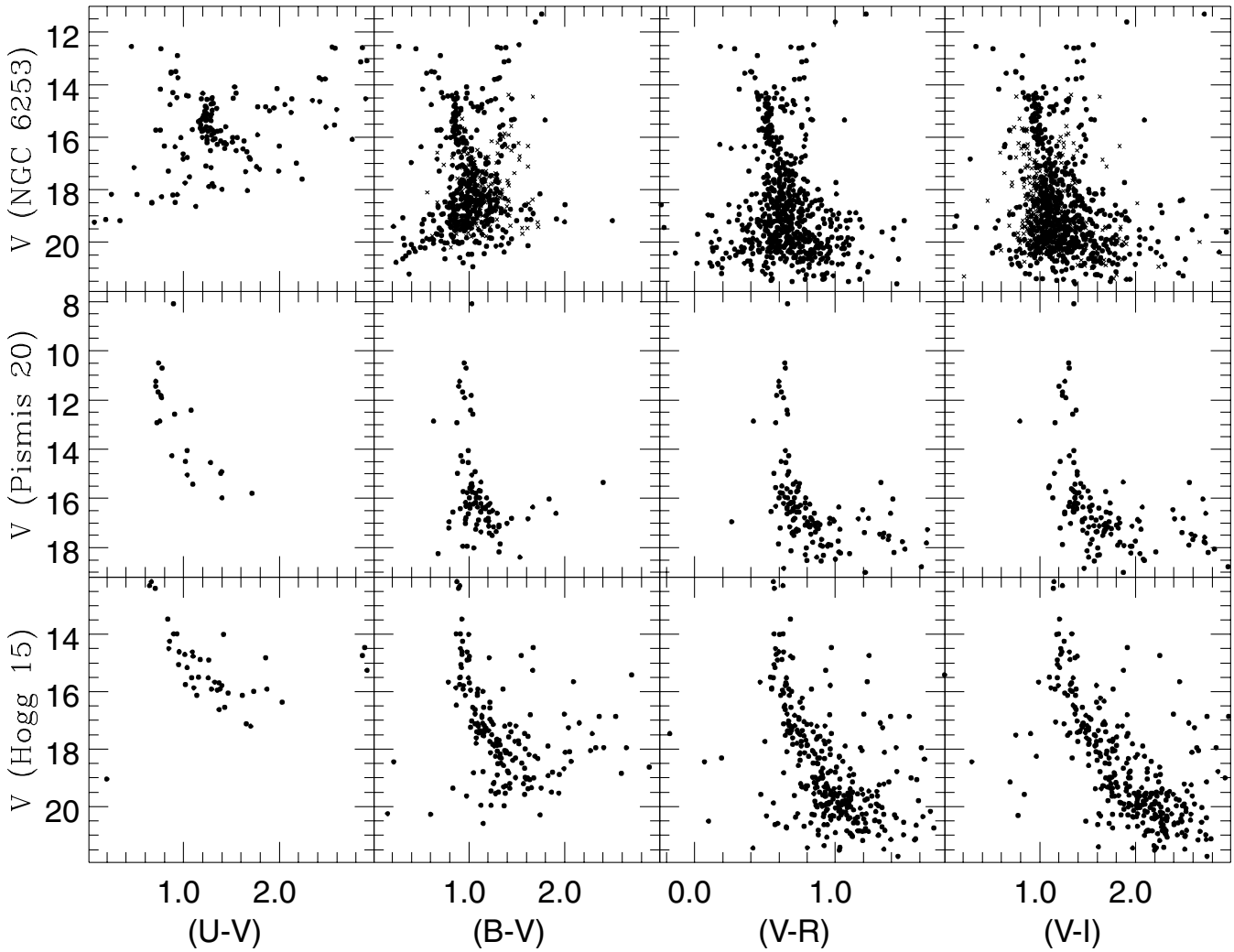

Figure 17. The $V, (U-V), V, (B-V), V, (V-R)$ and $V, (V-I)$ diagrams for the stars observed by us in the cluster (filled circles) and field (crosses) regions of Hogg 15, Pismis 20 and NGC 6253.

For the stars selected above, the $(B-V)_0, E(B-V)$ and $E(U-B)$ values have been determined using either the spectral type or the *UBV* photometric *Q* method (cf. Johnson & Morgan 1953; Sagar & Joshi 1979) with the calibration given by Schmidt-Kaler (1982). To calculate $E(V-R)$ and $E(V-I)$ values, we used the present $(V-R)$ and $(V-I)$ measurements, Sagar & Cannon's (1994) calibration between $(B-V)_0$ and $(V-R)_0$, and Walker's (1985) calibration between $(B-V)_0$ and $(V-I)_0$. To calculate $E(B-J), E(B-K)$ and $E(B-K)$ values, calibrations provided by Koornneef (1983) for the near-infrared colours have been used. The colour excess ratios derived in this way are listed in Table 14. They are in fair agreement with the normal values, indicating that the law of interstellar extinction in the direction of the clusters under discussion is normal. The mean values of colour excess $E(B-V)$ are listed in Table 15. For all clusters, our reddening estimates agree fairly well with the values estimated earlier by others (see Section 1), except in the case of Melotte 105. For the two older clusters, the reddening values are determined by fitting the theoretical isochrones in the CM diagrams. The distances and ages for all the objects under study are determined in the next section.

8 FITTING OF ISOCHRONES TO THE CM DIAGRAMS OF THE CLUSTERS

In order to determine distance moduli and ages of the clusters, we fit the theoretical stellar evolutionary isochrones given by either Bertelli et al. (1994) or Schaller et al. (1992) to the $V_0, (U-B)_0, V_0, (B-V), V_0, (V-R)_0$ and $V_0, (V-I)_0$ diagrams. To plot these figures, we have converted apparent *V* magnitude and $(B-V)$, $(U-B), (V-R)$ and $(V-I)$ colours into intrinsic ones using the values of $E(B-V)$ listed in Table 15 and the following relations for $E(U-B)$ (cf. Sagar & Joshi 1979), $E(V-R)$ (cf. Alcalá & Ferro 1988), A_v and $E(V-I)$ (Walker 1987):

$$E(U-B) = [X + 0.05E(B-V)]E(B-V),$$

where $X = 0.62 - 0.3(B-V)_0$ for $(B-V)_0 < -0.09$ and $X = 0.66 + 0.08(B-V)_0$ for $(B-V)_0 > -0.09$;

$$E(V-R) = [E1 + E2 \times E(B-V)]E(B-V),$$

where $E1 = 0.6316 + 0.0713(B-V)_0$ and $E2 = 0.0362 +$

Table 13. Frequency distribution of the stars in the $V, (V - I)$ diagram of the cluster and field regions. N_S,N_B and N_R denote the number of stars in a magnitude bin along, blueward and redward of the cluster sequence respectively. N_M (the difference between the N_S values of the cluster and field regions) denotes the statistically expected number of cluster members in the magnitude bin.

V range	Cluster region			Field region			Members	V range	Cluster region		
	N_B	N_S	N_R	N_B	N_S	N_R	N_M		N_B	N_S	N_R
				NGC 3105					Hogg 15		
12–14	0	4	2	0	2	0	2	12–13	0	3	0
14–15	0	7	2	0	4	0	3	13–14	0	3	0
15–16	0	14	3	0	3	4	11	14–15	0	10	2
16–17	0	21	1	0	9	4	12	15–16	0	16	3
17–18	0	23	3	0	14	12	9	16–17	0	16	3
				NGC 3603				17–18	2	46	5
10–12	0	3	0	0	0	0	3	18–19	2	36	5
12–13	1	6	0	1	0	0	6	19–20	2	81	5
13–14	2	16	0	1	0	0	16		Pismis 20		
14–15	3	26	1	2	0	0	26	8–10	0	1	0
15–16	13	34	1	7	2	0	32	10–11	0	2	0
16–17	6	47	4	6	2	1	45	11–12	0	5	0
17–18	24	70	1	23	2	0	68	12–13	1	3	0
				Melotte 105				13–14	0	0	0
11–12	0	3	1	0	1	0	2	14–15	0	6	0
12–13	0	8	3	0	1	0	7	15–16	0	18	2
13–14	0	12	3	0	0	0	12	16–17	0	31	8
14–15	1	35	0	0	1	1	34	17–18	0	32	11
15–16	0	25	2	0	2	2	23				
16–17	0	41	2	0	9	1	32				
17–18	0	39	1	1	14	3	25				
				NGC 4815							
10–12	0	2	0	0	0	0	2				
12–13	0	2	1	0	0	0	2				
13–14	0	7	3	0	1	2	6				
14–15	1	20	10	0	2	0	18				
15–16	1	61	6	0	6	3	55				
16–17	2	87	15	1	10	13	77				
17–18	3	95	27	1	33	14	62				
18–19	5	117	26	0	68	26	49				
				NGC 6253							
11–14	5	11	0	0	0	0	11				
14–15	1	27	6	0	1	2	26				
15–16	1	35	8	0	6	4	29				
16–17	5	31	4	3	14	12	17				
17–18	6	49	2	3	37	4	12				
18–19	7	111	8	3	76	2	35				
19–20	10	153	18	4	97	13	56				

$0.0078(B - V)_0$;

$$A_v = [3.06 + 0.25(B - V)_0 + 0.05E(B - V)]E(B - V)$$

and

$$E(V - I) = 1.25[1 + 0.06(B - V)_0 + 0.014E(B - V)]E(B - V).$$

We have used the same value of $E(B - V)$ for all the stars of a cluster region, and have not accounted for the presence of non-uniform extinction observed in the cluster regions (see previous section).

In order to define morphological features of the clusters in the CM diagrams accurately, and also for reliable estimation of distance moduli and ages of the clusters, we identify the stars of the inner ($R \leq 150$ pixel) and outer (remaining stars) regions in the cluster area. In deriving the cluster parameters, less weight is given to stars of the outer region and to obvious non-members. The uncertainty in distance and age determination is estimated from the errors in A_v and $E(B - V)$, and the errors in fitting the isochrones. The present determination of the distances to the clusters should be considered reliable because they have been derived by fitting the isochrones over a wide range of the unevolved part of the cluster MS.

Fitting of the isochrones has also been used to estimate the colour excesses for the two older clusters NGC 4815 and NGC 6253. The isochrones are derived from stellar models computed with the most recent radiative opacities, and include the effects of mass loss and convective core overshooting. The models are followed from the ZAMS to central carbon ignition for massive stars, and to the beginning of the thermally pulsing regime of the asymptotic giant branch phase for low- and intermediate-mass stars.

As the metallicity [Fe/H] values are not known spectroscopically for the clusters under study except for NGC 6253, we assumed that they have solar metallicity and used the isochrones computed for Population I stars ($X = 0.7$, $Y = 0.28$ and $Z = 0.02$). Analysis of the integrated light spectrum by Ahumada et al. (2000) and Santos & Bica (1993) also indicates metallicity similar to solar for Melotte 105 and Hogg 15 with [Fe/H] values of 0.0 ± 0.2 and -0.2 ± 0.2 respectively. For NGC 6253, high-resolution spectra of four giants

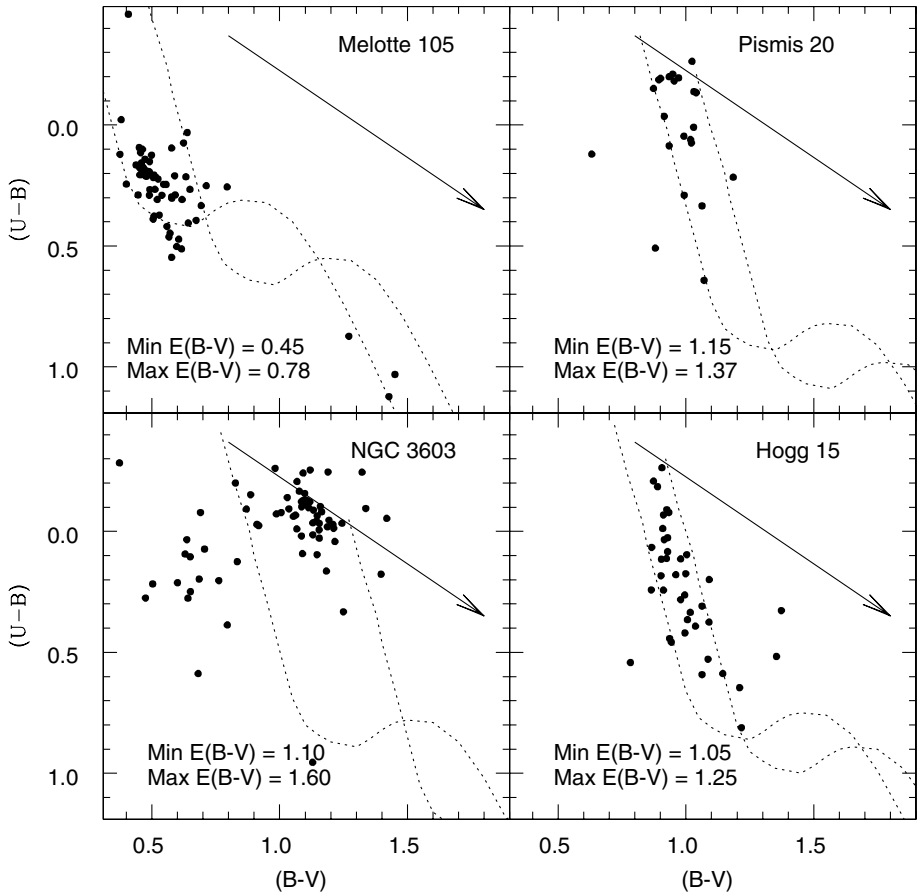

Figure 18. The $(U - B)$ versus $(B - V)$ diagrams for the stars observed in the cluster regions of NGC 3603, Melotte 105, Hogg 15 and Pismis 20. The continuous straight line represents the slope (0.72) as well as the direction of the reddening. The dotted curve represents the locus of the Schmidt-Kaler (1982) ZAMS shifted in the direction of reddening for the minimum (left-hand dotted curve) and maximum (right-hand dotted curve) values of $E(B - V)$ and $E(U - B)$ indicated in the diagram.

Table 14. A comparison of the colour excess ratios for star clusters with the corresponding values for the normal interstellar extinction law given by Schmidt-Kaler (1982) for $E(U - B)/E(B - V)$, by Alcalá & Ferro (1988) for $E(V - R)/E(B - V)$ and by Dean, Warren & Cousins (1978) for $E(V - I)/E(B - V)$. The values given by Mathis (1990) are also given for comparison where R and I wavelengths correspond to the Johnson system, while in the case of the normal interstellar medium (ISM), they correspond to the Cousins system.

Object	$\frac{E(U-B)}{E(B-V)}$	$\frac{E(V-R)}{E(B-V)}$	$\frac{E(V-I)}{E(B-V)}$	$\frac{E(B-H)}{E(B-J)}$	$\frac{E(B-K)}{E(B-J)}$
Normal ISM	0.72	0.65	1.25		
Mathis ISM	0.72	0.77	1.61	1.10	1.17
NGC 3105	0.77 ± 0.07	0.66 ± 0.05	1.22 ± 0.11		
NGC 3603	0.73 ± 0.01	0.68 ± 0.03	1.47 ± 0.03	1.13 ± 0.02	1.20 ± 0.04
Melotte 105	0.68 ± 0.01	0.35 ± 0.02	1.13 ± 0.05		
Hogg 15	0.74 ± 0.02	0.60 ± 0.03	1.32 ± 0.09		
NGC 4815	0.67 ± 0.04		1.32 ± 0.11		
Pismis 20	0.75 ± 0.03	0.62 ± 0.04	1.35 ± 0.06		
NGC 6253	0.70 ± 0.05	0.75 ± 0.06	1.35 ± 0.10		

indicate [Fe/H] $= 0.36 \pm 0.15$ (cf. Carretta et al. 2000). We have therefore used the Bertelli et al. (1994) isochrones corresponding to $Z = 0.05$ for this cluster.

The intrinsic CM diagrams for NGC 3105, NGC 3603, Hogg 15 and Pismis 20 are presented in Fig. 19, while those for Melotte 105, NGC 4815 and NGC 6253 are shown in Fig. 20. As most of the factors responsible for the colour spread in the MS will redden the stars, we have used, as far as possible, the blue envelope of the MS with due allowance for the colour spread expected from the observational errors and non-uniform extinctions in CM diagrams. The cluster parameters determined in this way, along with the Hertzsprung–Russell (HR) diagram, are described below.

NGC 3105. We present the first CCD *BVRI* data for this cluster. As the *U* data are useful for the study of young stars, they have been taken from the photoelectric photometry of FitzGerald et al.

Table 15. Parameters derived for the clusters under study. To determine the Galactocentric distance, R_G, to a cluster, a value of 8.8 kpc has been assumed for the Galactocentric distance of the Sun. The numbers of red giants, blue supergiants, blue stragglers and WR stars in the clusters have been denoted by N_R, N_S, N_B and N_W respectively. The values of colour excesses and distance moduli are given in magnitudes. The MF slopes x_1 and x_2 are derived from the LFs $N1$ and $N2$ respectively.

Parameter	NGC 3105	NGC 3603	Melotte 105	Hogg 15	NGC 4815	Pismis 20	NGC 6253
$E(B-V)$	1.06	1.44	0.52	1.15	0.72	1.20	0.20
(V_0-M_V)	14.9 ± 0.3	14.3 ± 0.3	11.8 ± 0.2	12.4 ± 0.2	12.2 ± 0.15	12.75 ± 0.2	11.3 ± 0.15
Distance (kpc)	9.5 ± 1.5	7.2 ± 1.2	2.3 ± 0.2	3.0 ± 0.3	2.75 ± 0.2	3.55 ± 0.35	1.8 ± 0.12
R_G (kpc)	11.8	9.1	8.2	7.6	7.6	6.5	7.2
Z (pc)	46	−65	−98	−13	−100	−75	−196
Age (Myr)	25 ± 10	3 ± 2	250 ± 30	6 ± 2	400 ± 50	6 ± 2	2500 ± 600
N_R	0	0	6	0	15	0	24
N_S	5	8	0	1	0	2	0
N_B	1	1	1	1	2	1	5
N_W	0	5	0	1	0	1	0
MF slope (x_1)	0.5 ± 1.7	0.84 ± 0.05	1.15 ± 0.28		1.40 ± 0.7		
MF slope (x_2)	0.2 ± 0.9	0.86 ± 0.04	1.45 ± 0.24	1.35 ± 0.21	2.2 ± 0.5	1.0 ± 0.2	
Mass range ($M_\odot$)	10.6−5.8	75−7	3.7−1.1	19−1.2	3.1−1.1	30−2.2	

(1977) only for the probable cluster members. The *BV* photoelectric data for the cluster members not observed by us have also been adopted from FitzGerald et al., since they are very important for estimating the cluster age and also for the study of the stellar evolutionary status of the cluster. The unevolved MS of the cluster has been observed for the first time. The MS is spread over 3 mag in V (see Fig. 19). There are five supergiants as possible cluster members. One of the stars not observed by us has been indicated as a blue straggler member of the cluster by Ahumada & Lapasset (1995). The Bertelli et al. (1994) theoretical isochrones fitted to the bright evolved stars and also to the unevolved cluster MS are overplotted. This yields $(V_0-M_V)=14.9$ mag as the distance modulus and 25 Myr as the age. It was noticed that the theoretical isochrones can be fitted to the brighter stars for a range of distance moduli and ages. However, spectroscopic information available for the brighter stars is used to decide their evolutionary status and thereby put constraints on the cluster age. The distance modulus and age determinations therefore have relatively large uncertainty, with values of 0.3 mag and 10 Myr respectively. The present age estimate and the reddening value agree fairly well with earlier estimates given by Moffat & FitzGerald (1974) and FitzGerald et al. (1977). However, our distance estimate of 9.5 ± 1.5 kpc puts the cluster farther than the value of 5.5 kpc given by FitzGerald et al. (1977), but is consistent with the value of 8.0 ± 1.5 kpc given by Moffat & FitzGerald (1974). The present distance determination should be reliable as we have been able to identify unambiguously the unevolved cluster MS, unlike other studies where only an evolved cluster sequence was observed. The present distance determination coupled with the young age makes NGC 3105 a valuable object for spiral structure and galactic dynamics studies, as it becomes one of the farthest known young star clusters in our Galaxy. In order to put the present distance determination on a stronger footing, spectroscopic as well as radial velocity measurements of some brighter members are needed.

NGC 3603. The intrinsic CM diagram of NGC 3603 (see Fig. 19) is generated from the present *UBVRI* data using the $E(B-V)$ value listed in Table 15. The foreground stars clearly seen in the apparent CM diagrams (Fig. 16) are not plotted here. *RI* photometric data for the cluster region have been obtained for the first time. Both photometric and spectroscopic observations from the ground as well as with *HST* indicate the presence of about 50 O-type stars. Of these, several are actually supergiants and WR stars. Ahumada & Lapasset (1995) have classified a star of spectral type O5.5 III(f) as a blue straggler. A distance modulus $(V_0-M_V)=14.3\pm0.3$ mag has been derived for NGC 3603 using the spectral classifications of stars published in the literature, as the present photometric diagram cannot be used for this purpose because of its extremely young age. A cluster sequence with large scatter mostly resulting from differential extinction can be seen in the diagrams. An isochrone of 3 Myr taken from Schaller et al. (1992) is shown in the diagrams. Earlier studies by Melnick et al. (1989) and Moffat et al. (1994) and more recently by Eisenhauer et al. (1998) indicate that all high-mass stars in the cluster did not form at the same time but spread over a period of about a few Myr.

Hogg 15. The $V_0,(U-B)_0$, $V_0,(B-V)_0$, $V_0,(V-R)_0$, and $V_0,(V-I)_0$ diagrams for Hogg 15 generated from the present *UBVRI* data are shown in Fig. 19. As CCD observations could not be carried out for the WR star HDE 311884, the brightest probable cluster member, its photoelectric *UBV* data are taken from Moffat (1974a). Such deep CCD CM diagrams for Hogg 15 are presented for the first time. They are about 4.5 mag fainter than those given by Moffat (1974a). A well-defined cluster MS spreading over 4 mag is clearly seen. The MS turn-off point is not clearly defined. These, along with the presence of a WR star and non-uniform extinction in the cluster, indicate that the cluster is extremely young, like NGC 3105 and NGC 3603 of our sample. The Bertelli et al. (1994) theoretical isochrones have been fitted to the unevolved cluster MS and to the bright stars (see Fig. 19). This yields a value of 12.4 ± 0.2 mag for (V_0-M_V) and 6 ± 2 Myr for the cluster age. The very close location of the WR star to the isochrone in the $V_0,(U-B)_0$ and $V_0,(B-V)_0$ diagrams seems to confirm its cluster membership. In fact, Ahumada & Lapasset (1995) have classified it as a blue straggler. The cluster parameters determined here agree very well with those given earlier by Moffat (1974a).

Pismis 20. The $V_0,(U-B)_0$, $V_0,(B-V)_0$, $V_0,(V-R)_0$, and $V_0,(V-I)_0$ diagrams shown in Fig. 19 for Pismis 20 are based on the present *UBVRI* data. *I* data for the cluster are presented for the first time. We confirm the features of the CM diagrams observed earlier by Vázquez et al. (1995). The cluster has a few O- and B-type giant and supergiant members. The location of the brightest star in Fig. 19 indicates that it could be a blue straggler member of the cluster. A well-defined cluster sequence over a V magnitude range of 7 is clearly visible. The radial velocity measurements of the brightest star HD 134959 in the CM diagrams, having spectral type of B2 Ia-O, confirm its cluster membership. The star WR 67 of

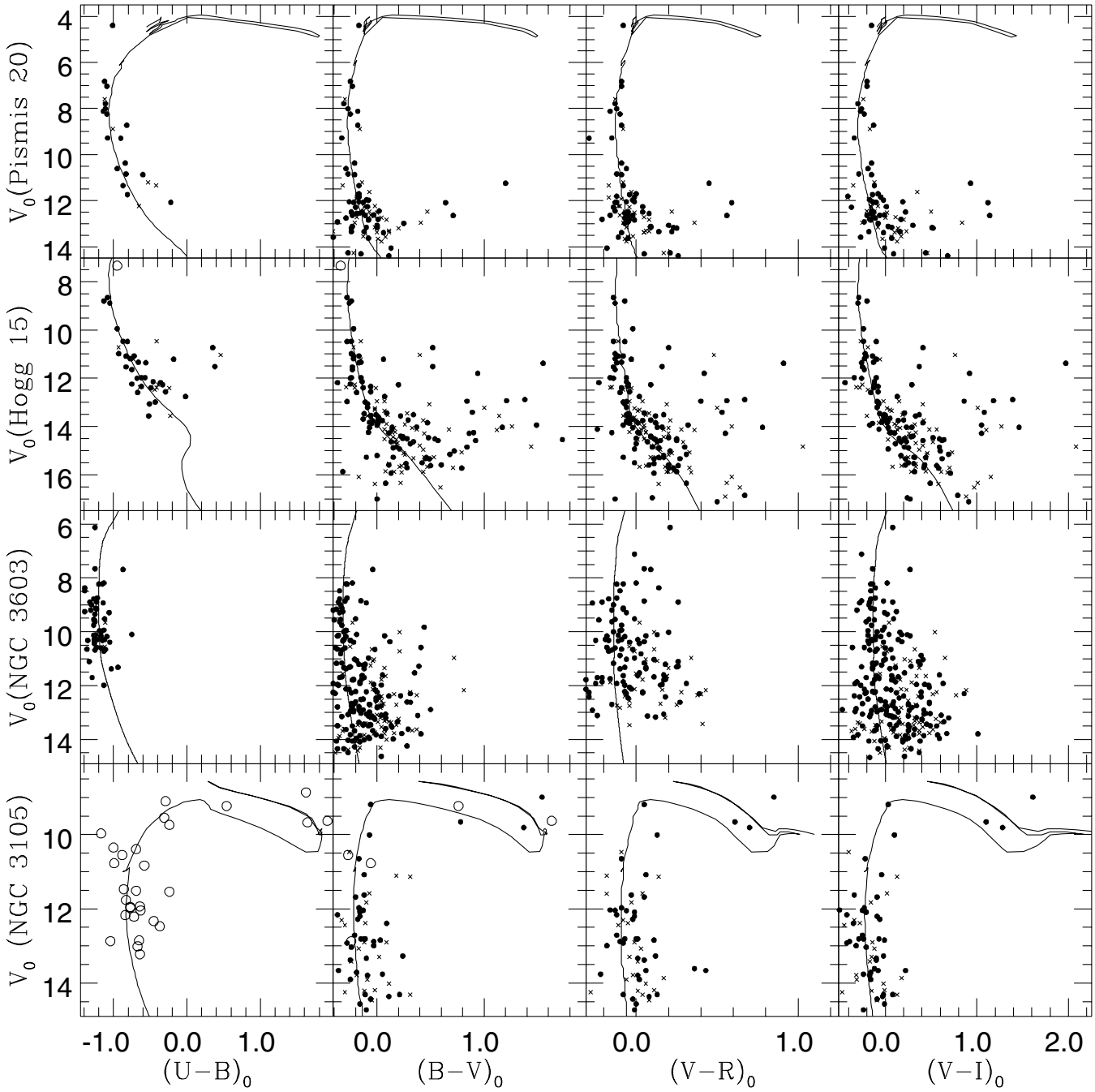

Figure 19. The $V_0, (U-B)_0, V_0, (B-V)_0, V_0, (V-R)_0$ and $V_0, (V-I)_0$ diagrams for stars of the inner (filled circles) and outer (crosses) regions in the young clusters NGC 3105, NGC 3603, Hogg 15 and Pismis 20. Open circles in NGC 3105 and Hogg 15 denote probable members observed photoelectrically in *UBV* passbands by FitzGerald et al. (1977) and Moffat (1974a) respectively. The continuous curves are the isochrones given by Bertelli et al. (1994) (except in NGC 3603 where it is by Schaller et al. 1992) for solar metallicity fitted to the data set. The derived values of $(V_0 - M_V)$ and log(age) are 14.9 and 7.4 for NGC 3105, 14.3 and 6.5 for NGC 3603, 12.4 and 6.8 for Hogg 15 and 12.75 and 6.8 for Pismis 20.

spectral type WN6 is also a member. All these, combined with the almost vertical cluster MS in the CM diagrams, indicate that the cluster is extremely young and joins the group of NGC 3105, NGC 3603 and Hogg 15 amongst the clusters under study. The MS turn-off point has colour $(B-V)_0 = -0.30$ mag. The Bertelli et al. (1994) isochrones fitted to the cluster sequence indicate that the cluster age is 6 ± 2 Myr and $(V_0 - M_V) = 12.75 \pm 0.2$ mag. The present determination of cluster parameters agrees, within errors, very well with the recent determinations by Turner (1996) and Vázquez et al. (1995). However, the present distance is larger by a factor of about 1.6 compared with that given by Moffat & Vogt (1973). This may be due to the fact that the latter determination is based on only a handful of relatively brighter stars. The location of the extremely young cluster Pismis 20 makes it valuable for the study of spiral structure in the Norma–Scutum arm of the Galaxy.

Melotte 105. The $V_0, (U-B)_0, V_0, (B-V)_0, V_0, (V-R)_0$, and $V_0, (V-I)_0$ diagrams for Melotte 105 have been plotted in Fig. 20

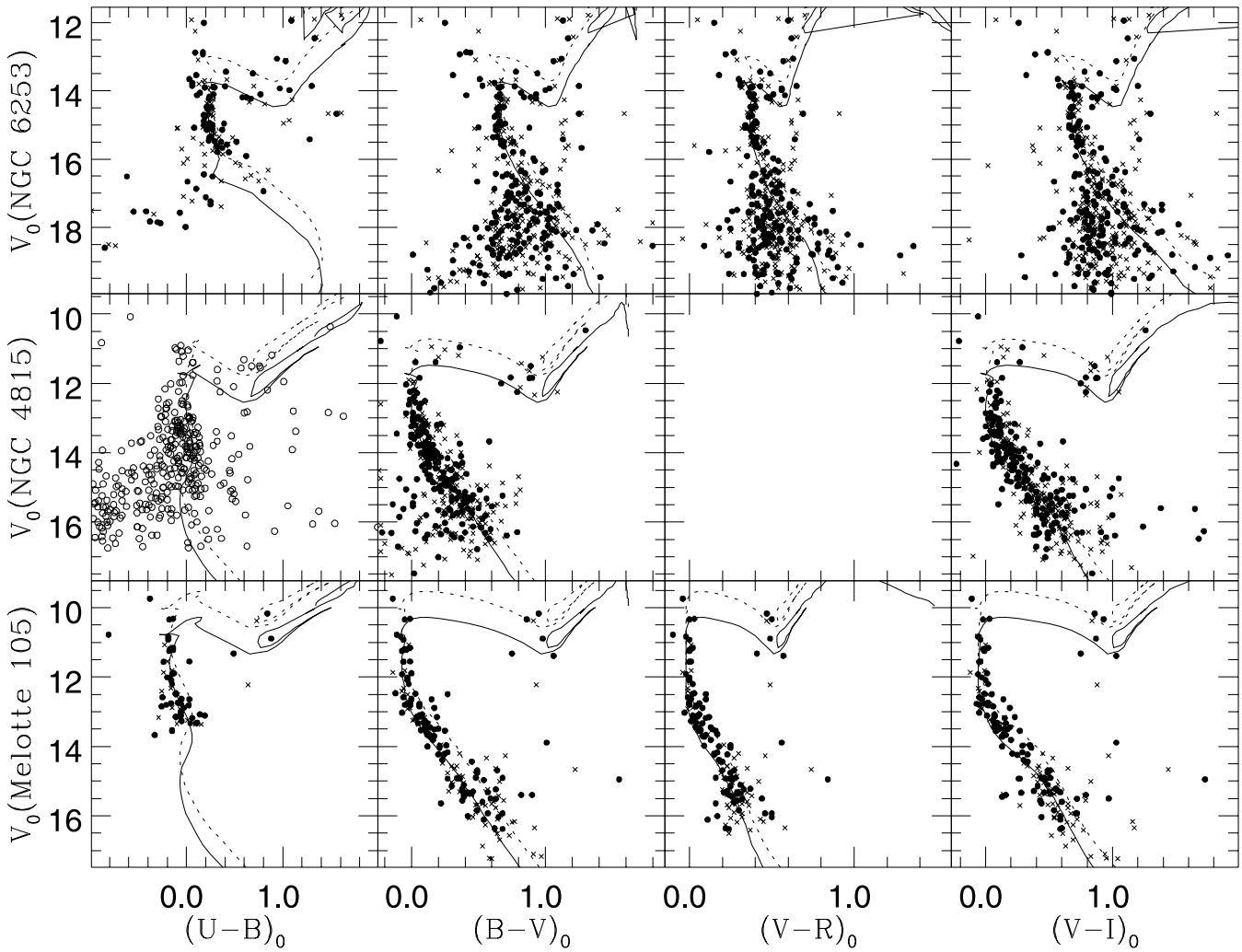

Figure 20. The $V_0, (U-B)_0$, $V_0, (B-V)_0$, $V_0, (V-R)_0$ and $V_0, (V-I)_0$ diagrams for stars of the inner (filled circles) and outer (crosses) regions in Melotte 105, NGC 4815 and NGC 6253. In NGC 4815, the $V_0, (U-B)_0$ diagram is based on data (open circles) from Kjeldsen & Frandsen (1991). The continuous curves are the isochrones given by Bertelli et al. (1994) for solar metallicity, except in NGC 6253 where the Z value is 0.05 (see text), fitted to the data set. The derived values of $(V_0 - M_V)$ and log(age) are 11.8 and 8.4 for Melotte 105, 12.2 and 8.6 for NGC 4815 and 11.3 and 9.4 for NGC 6253. The dotted curves show the extent to which binaries of equal mass can brighten the isochrones of single stars.

using the present *UBVRI* data. The *RI* data for the cluster have been obtained for the first time. A well-defined cluster MS spreading over 4 mag is clearly seen, except in the $V_0, (U-B)_0$ diagram. Brighter stars show stellar evolutionary effects and a few have already reached the red giant phase. The present photometry is more than a magnitude deeper than that of Kjeldsen & Frandsen (1991). We confirm their observed stellar evolutionary features for the cluster. The fitting of Bertelli et al. (1994) isochrones to the bright evolved stars along with an unevolved cluster MS yields $(V_0 - M_V) = 11.8 \pm 0.2$ mag and an age $= 250 \pm 30$ Myr for the cluster. The extent to which binaries of equal mass brighten the isochrone of single stars is also shown. The brightest star above the MS turn-off point (see Fig. 20) in all CM diagrams occupies the position of blue straggler, as is also indicated by Ahumada & Lapasset (1995). The present values of distance, age and reddening are in excellent agreement with those determined by Kjeldsen & Frandsen (1991). However, both our age and $E(B-V)$ values are larger than the corresponding values of 100 Myr and 0.31 ± 0.02 mag as derived by Ahumada et al. (2000) using the integrated light spectrum of the cluster. The present reddening determination is also larger than the values given by Sher (1965) and Balona & Laney (1995), while the age estimates are similar. Our values fit best to the data.

NGC 4815. For this cluster only *BVI* CCD photometric observations have been carried out by us. The $V_0, (B-V)_0$ and $V_0, (V-I)_0$ diagrams for NGC 4815 are therefore generated from the present data, while for the $V_0, (U-B)_0$ diagram the data are borrowed from Kjeldsen & Frandsen (1991). They are shown in Fig. 20. We have thus used all the available data in the literature to determine reliable cluster parameters. In all the CM diagrams the MS turn-off points in addition to well-developed giant branches can be clearly identified in spite of the presence of field star contamination in the diagrams. The overall morphology of the CM diagrams indicates that NGC 4815 is an intermediate-age cluster. Since stars of spectral types earlier than A0 have evolved off the MS, the reddening could not be determined using the $(U-B)$,

$(B-V)$ diagram. The reddening, distance modulus and age of the cluster have been determined by fitting the Bertelli et al. (1994) solar metallicity isochrones to the cluster sequence present in the different CM diagrams. The values in magnitudes determined in this way are $E(U-B)=0.48$, $E(B-V)=0.72$, $E(V-I)=0.95$, $(V_0-M_V)=12.2$ and a cluster age of about 400 Myr. Within the errors, these parameters agree fairly well with the earlier determinations by Kjeldsen & Frandsen (1991) and by Carraro & Ortolani (1994). An inspection of Fig. 20 reveals 15 red giants and two blue stragglers as probable cluster members. The photometric values obtained by us for star 8692 of the cluster region (see Table 8) are $(V-I)=5.8$, $(B-V)=2.32$ and $V=16.39$ mag. For the same star, Kjeldsen & Frandsen (1991) measured $V=16.14$, $(B-V)=2.40$ and $(U-B)=-0.47$ mag, while Carraro & Ortolani (1994) obtained $V=16.47$ and $(B-V)=2.35$ mag. The star is thus peculiar in the sense that it has an extremely red colour along with a blue ultraviolet colour. It could be an interacting binary, as such stars have extreme red colours with an ultraviolet excess (cf. Munari et al. 1992). Further observations are desired to understand the nature of the star.

NGC 6253. The $V_0,(U-B)_0$, $V_0,(B-V)_0$, $V_0,(V-R)_0$, and $V_0,(V-I)_0$ diagrams for NGC 6253 are shown in Fig. 20. They are generated from the present *UBVRI* data. The colour excesses are $E(U-B)=0.14, E(B-V)=0.20, E(V-R)=0.15$ and $E(V-I)=0.27$ mag. They are estimated by fitting the isochrones of an age to the observed CM diagrams, keeping the cluster at the same distance. We confirm the features of an old star cluster as reported earlier by Bragaglia et al. (1997) and Piatti et al. (1998). However, in comparison with these studies, the cluster MS and the subgiant and redgiant branches are better defined by our data, especially for stars brighter than $V_0=16$ mag. This is most probably due to the fact that our observations are only for the central region of the cluster. The effects of field star contamination in stars brighter than $V_0\sim16$ mag are therefore reduced (see Fig. 20). With the fainter stars, the cluster MS cannot be separated from the field stars. In agreement with earlier investigators, we conclude the presence of strong field star contamination in the direction of the cluster.

High-resolution spectroscopic measurements yield a value of $[\mathrm{Fe/H}]=0.36\pm0.15$ for the metallicity of the cluster (Carretta et al. 2000). We have therefore used the Bertelli et al. (1994) isochrones for $Z=0.05$ to estimate the cluster parameters. The cluster sequence has a clearly defined MS turn-off point. Some blue stragglers along with well-developed giant branches and red clumps are also clearly seen in the CM diagrams. The best-fitting isochrone has been overplotted in Fig. 20. The extent to which binaries of equal mass can brighten the isochrones of single stars is also shown. The values of the true distance modulus and age determined in this way are 11.3 ± 0.15 mag and 2.5 ± 0.6 Gyr respectively. Within the errors, the cluster parameters determined by us agree fairly well with the recent determinations by Bragaglia et al. (1997) and Piatti et al. (1998). Out of 44 red giants observed by Bragaglia et al. (1997), only half of them are located in the region imaged by us. The locations of at least five stars in Fig. 20 indicate that they may be blue straggler cluster members.

Table 15 indicates that WR stars and blue supergiants are present only in extremely young (age <10 Myr) star clusters; red giants are present in clusters older than 20 Myr but blue stragglers are present in clusters of all ages.

9 LUMINOSITY AND MASS FUNCTIONS OF THE CLUSTERS UNDER STUDY

The LF, defined as the variation in stellar counts per unit magnitude range, can in principle be derived from observations in one wavelength band only. However, from such data, it is not possible to distinguish MS stars from evolved red giants and other non-MS stars. The latter play an important role in the construction of LFs for star clusters that are superimposed on fields composed of a significantly varied mix of stellar populations, as can be seen from the present observations of NGC 4815 and NGC 6253 plotted in Figs 16 and 17 respectively. Two colours, such as *B* and *V* or *V* and *I*, are required for their identification. It is therefore necessary to construct the MS LF either from a $V,(B-V)$ or from a $V,(V-I)$ diagram instead of from a single *B* or *V* or *I* band. We preferred the $V,(V-I)$ diagram over the $V,(B-V)$ one as it is generally deeper (at least by a magnitude). The LFs of star clusters and their corresponding field regions are generally determined from star counts in bin widths of 1 mag in *V* by including only stars located in the cluster MS region. As some clusters under study have differential extinction across the cluster region, the widening of the cluster MS owing to extinction as well as photometric errors, binaries, etc., has been considered. The brighter magnitude limit of the LF has been decided from the stellar evolutionary effects, while the fainter one has been decided from the data completeness limit which is generally $V\sim18$, about 2 mag above the data limit. The cluster regions under investigation are not crowded except for NGC 3603, and the use of the DAOPHOT artificial 'star add' technique by Carraro & Ortolani (1994) for NGC 4815, by Bragaglia et al. (1997) for NGC 6253 and by Sagar & Griffiths (1998b) for a few other open star clusters indicates that the data are generally more than 90 per cent complete for the brightness of the stars considered here. We have therefore considered it unnecessary to perform Monte Carlo simulations using the DAOPHOT 'star add' technique, and assumed that the results derived here are not affected by the data incompleteness problem. In the case of NGC 3603, we have avoided the most crowded central part of the cluster, because, owing to the density, high-resolution ground-based (see Hofmann et al. 1995; Eisenhauer et al. 1998) or *HST* (see Moffat et al. 1994; Drissen et al. 1995) observations are required. The results of the LF analysis derived in this way are listed in Table 16. The field star contamination generally increases with decreasing brightness as expected. It is largest for NGC 4815. The population of the field stars for NGC 3603 and NGC 6253 seems to be clearly separated from the cluster sequence, and appears to come mostly from the foreground for NGC 3603 and from the background for NGC 6253. The field star contamination estimated from the present data agrees, within errors, with those derived by Carraro & Ortolani (1994) for NGC 4815 and by Bragaglia et al. (1997) for NGC 6253, who had in all cases different field regions.

A mass–luminosity relation is needed to convert a cluster LF into an MF. For this, we used the values of reddening $E(B-V)$, distance and age for the clusters given in Table 15. The theoretical stellar evolutionary isochrones used for the age estimation have also been used to convert luminosity into mass in the present analysis.

9.1 Slope of the MFs

To convert the LFs into MFs, we divide the numbers given in Table 16 by the mass interval, ΔM, of the magnitude bin under consideration. The value of ΔM was obtained from the

Table 16. The luminosity and mass functions for the clusters under study. M denotes the mass in $M_\odot$ corresponding to the V magnitude of the bin centre. The raw counts for the LFs of cluster and field regions derived for the cluster MS population present in the corresponding $V,(V-I)$ diagrams are denoted by NC and NF respectively. After the correction of field star contamination and division by the mass interval, ΔM, of the V magnitude bin under consideration NC yields $N1$; while NC gives $N2$ if we divide it only by ΔM assuming no field star contamination in the cluster region.

Cluster	Range in V mag	$M(M_\odot)$	NC	NF	$N1$	$N2$
NGC 3105	13–14	10.0	4	2	3.16	6.31
	14–15	9.6	9	2	8.03	10.32
	15–16	8.4	17	3	9.58	11.64
	16–17	6.7	22	7	7.86	11.53
NGC 3603	10–12	72.3	3	0	0.34	0.34
	12–13	58.8	6	0	0.45	0.45
	13–14	43.8	16	0	1.01	1.01
	14–15	29.2	26	0	1.97	1.97
	15–16	18.5	34	2	3.92	4.17
	16–17	12.0	47	2	9.27	9.69
	17–18	8.0	70	2	20.22	20.81
Melotte 105	12–13	3.5	8	1	12.57	14.37
	13–14	2.9	12	0	18.80	18.80
	14–15	2.3	35	1	57.86	59.56
	15–16	1.8	25	2	61.41	66.75
	16–17	1.4	41	9	102.53	131.37
	17–18	1.2	39	14	126.94	198.03
Hogg 15	12–13	16.4	3			0.66
	13–14	11.8	3			0.71
	14–15	8.5	10			2.87
	15–16	5.7	16			7.60
	16–17	3.6	16			10.28
	17–18	2.5	46			48.50
	18–19	1.7	36			54.80
	19–20	1.5	81			275.32
NGC 4815	14–15	2.9	20	2	26	28.89
	15–16	2.3	61	6	106.14	117.72
	16–17	1.7	87	10	251.14	283.75
	17–18	1.4	95	33	195.59	299.70
	18–19	1.2	117	68	249.09	594.77
Pismis 20	8–10	27.4	1			0.27
	10–11	24.8	2			0.59
	11–12	20.5	5			1.21
	12–13	16.4	3			0.66
	14–15	8.5	6			1.72
	15–16	5.7	20			9.55
	16–17	3.6	39			25.12
	17–18	2.5	43			45.50
NGC 6253	14–14.5	0.90	9	1	437.55	492.25
	14.5–15	0.88	18	0	984.50	984.50
	15–15.5	0.86	18	1	929.80	984.50
	15.5–16	0.84	18	3	820.42	984.50
	16–16.5	0.82	19	4	820.42	1039.19
	16.5–17	0.80	12	8	218.78	656.33

mass–luminosity relation derived from the appropriate isochrone. The resulting cluster MFs in the case of LFs represented by $N1$ are plotted in Fig. 21, and the values of MF slopes are given in Table 15. The slope has been derived from the mass distribution, $\xi(M)$. If dN denotes the number of stars in a bin with central mass M, then the value of x is determined from the linear relation

$$\log(\mathrm{d}N) = -(1+x)\times\log(M) + \text{constant}$$

using a least-squares solution. The errors given in Table 15 are formal errors resulting from the linear regression to the data points.

In order to study the changes in the MF slopes arising from field stars, we derive two MF slopes, namely x_1 and x_2, from the LFs given by $N1$ and $N2$ respectively (see Table 16). This indicates that the two MF slopes agree within the errors. However, in general, except for NGC 3105, the MF becomes steeper when field star correction is not applied. The extent of steepening is related to the amount of field star contamination, as expected. This clearly demonstrates the importance of correction for field star contamination in the MF analysis. We have considered the values of x_1 for NGC 3105, NGC 3603, Melotte 105 and NGC 4815 and of x_2 for Hogg 15 and Pismis 20 because there is no field region observed for them as a representative of the cluster MF slopes, and will use them in our further discussions.

It is worth mentioning here that Eisenhauer et al. (1998) derived a MF slope of ~0.73 down to 1 $M_\odot$ for the central region of NGC 3603 using near-infrared (*JHK*) data obtained with adaptive optics imaging. They accounted for both data incompleteness and field

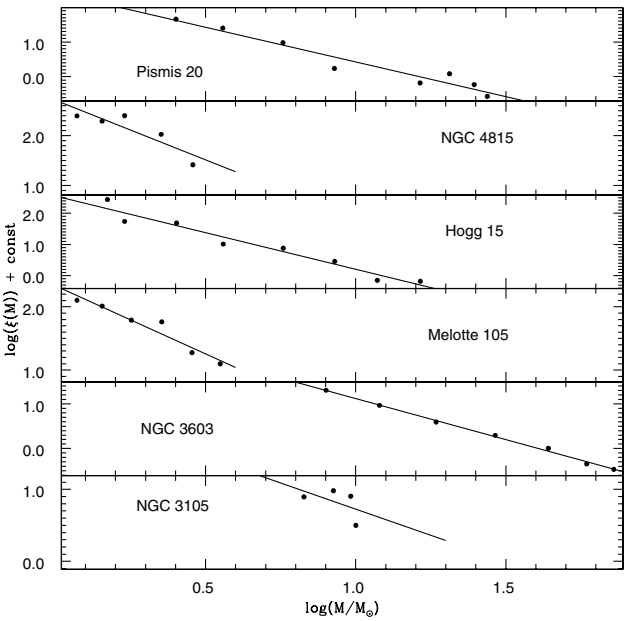

Figure 21. Plot of the mass functions derived from the LF corrected for field star contamination except for Hogg 15 and Pismis 20. Inclined solid lines show the MF slope determined from the least-squares linear solutions.

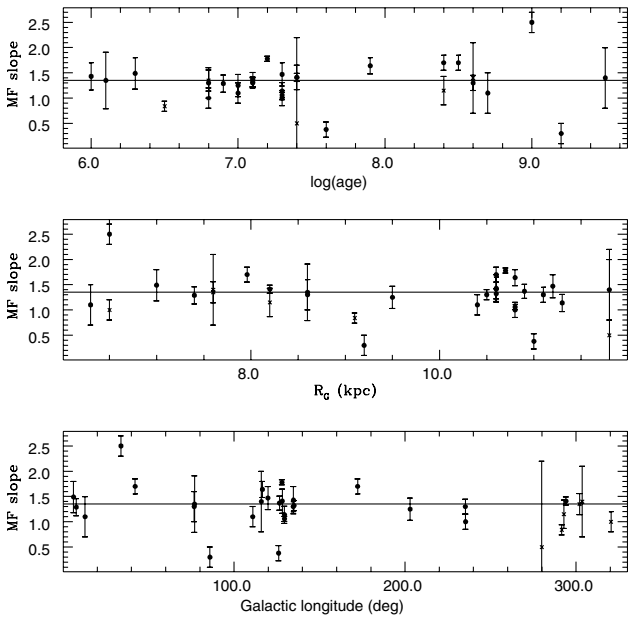

Figure 22. Dependence of the mass function slope on the Galactic longitude, Galactocentric distance, R_G and the age of the star cluster. Data taken from Sagar (2000) and the present work are denoted by filled circles and crosses, respectively. The horizontal lines represent the value of the Salpeter slope. The three clusters having MF slopes most deviant from the Salpeter value are NGC 436, NGC 7044 and Berkeley 81 with log(age) values of 7.6, 9.2 and 9.0 respectively.

star contamination. Their value agrees fairly well with our value (0.84 ± 0.05) of MF slope for the cluster. However, for mass $\geq 15\,M_\odot$, they derive a MF slope of 1.7. This agrees with the values of 1.59 ± 0.22 and 1.4 ± 0.6 derived for the central region of NGC 3603 by Hofmann et al. (1995) and Moffat et al. (1994) respectively. On the other hand, the present study is mainly for the regions outside the central core which could not be resolved by our ground-based observations. The present MF for mass $\geq 15\,M_\odot$ has a slope of 0.88 ± 0.1, somewhat flatter than the slope observed in the central core.

Vázquez et al. (1995) derive a value of 1.04 for the MF slope of Pismis 20, which is exactly the value obtained by us. For NGC 4815, Carraro & Ortolani (1994) derive a MF slope of 1.55 ± 0.20. They corrected the star counts for both data incompleteness and field star contamination. Recently, Chen et al. (1998) determined a value of 1.2 ± 0.3 as a slope of the NGC 4815 MF in the mass range of 1.5 to $2.3\,M_\odot$ by carefully separating cluster members from field stars. As both determinations agree very well with our value of 1.40 ± 0.7 for NGC 4815, our earlier assumption about data completeness in deriving the present LF appears to be justified.

Because of its extremely old age, the NGC 6253 data cover only a very narrow mass range (see Table 16) and thus are not useful for the MF study, although the data indicate that in such a narrow mass range the MF is not an increasing one. This is similar to the MFs of a number of old (2–6 Gyr) open clusters, including Berkeley 32 (see Richtler & Sagar 2001, and references therein).

9.2 Discussion of the MF slopes

Except for the cluster NGC 3105 of the sample, the MF slopes are not significantly different from the Salpeter (1955) value of 1.35 in the solar neighbourhood. The steepest and flattest values are 1.40 and 0.84 for NGC 4815 and NGC 3603 respectively. In the sample studied for MFs, they are the oldest and youngest objects respectively. This indicates that, above $1\,M_\odot$, MF slopes of young ($<$500 Myr) star clusters seem to be similar to the Salpeter MF in the solar neighbourhood.

The present determination, along with the previous reliable estimates of MF slope above $1\,M_\odot$ (see Sagar 2000) for individual objects, has been used to study the dependence of the MF slope, x, on the Galactic longitude, Galactocentric distance, R_G, and age of the star clusters. The distance and age of these objects are taken from their respective studies (cf. Sagar 2000). In converting geocentric distance to Galactocentric distance, R_G, the distance between the Sun and the Galactic Centre is taken as 8.8 kpc. Fig. 22 shows the plot of x versus Galactic longitude, R_G and cluster age. The clusters are located in different parts of the Galaxy, as the Galactic longitude varies from about 0° to 330°. The range in R_G is from 6 to 12 kpc, while the ages of clusters range from 1 to 3200 Myr. The value of the Salpeter (1955) slope is shown as a straight line in Fig. 22. The values of MF slopes of clusters younger than about 500 Myr seem to have no dependence on Galactic longitude, R_G or cluster age, and all, within a 1σ error, agree with the Salpeter value. In older clusters, dynamical evolution can change the shape of the IMF, and we might anyway not expect the IMF to be still realized from the observed MFs of such clusters. As a cluster evolves dynamically, low-mass stars evaporate out of the cluster potential faster than high-mass stars. In a cluster much older than its relaxation time, the dynamical effect therefore can change an originally rising IMF into a flat or even declining MF. However, there are also old clusters with MFs indistinguishable from a Salpeter MF: e.g. Berkeley 99 (age 3.2 Gyr) has MF slope of $\sim$1.4 (Sagar & Griffiths 1998b).

While no systematic variation of x with Galactic longitude, R_G or cluster age is detectable in Fig. 22, there is a scatter of $\sigma_x = 0.3$ dex around the Salpeter value. Piskunov (1976) analysed the MF slopes of 61 open star clusters and found an average value of

$x = 1.3 \pm 0.3$ in the mass range of 1 to 25 $M_\odot$. Similarly, in five young and well-populated open clusters, Sagar et al. (1986) derive an average value of $x = 1.4 \pm 0.2$ within the mass range of 1.3 to 80 $M_\odot$. Recently, using data from CCD observations of 13 and 8 star clusters, Kjeldsen & Frandsen (1991) and Phelps & Janes (1993) derived average MF slopes of 1.3 ± 0.2 and 1.4 ± 0.3 respectively. For some more young star clusters, Subramaniam & Sagar (1999) and Sanner & Geffert (2001) determined average values of $x = 1.4 \pm 0.3$ and 1.8 ± 0.6 respectively for the MF slope above 1 $M_\odot$. In order to answer the question of possible variations in MF slopes, it is necessary to know the accuracy of MF determination in young Galactic star clusters. The inherent uncertainty in such a determination is due to scatter introduced by Poisson noise, unresolved binaries and the dynamical and stellar evolution of the star clusters. Recently, Kroupa (2001) has investigated them theoretically using techniques of numerical simulation and found that, in the MF slope determination of Galactic star cluster type objects, they introduce a scatter of $\sigma_x \sim 1$ above 1 $M_\odot$. Uncertainties in corrections of field star contamination and data incompleteness will further increase the scatter [see discussions in Sagar & Richtler (1991) and Sagar & Griffiths (1998b)]. All these clearly indicate that the MF slope of young star clusters, and hence the IMF based on them, can never be determined more accurately than this scatter, and that the scatter seen in Fig. 22 and also observed by other investigators mentioned above can be explained with Poisson noise and dynamical effects.

10 CONCLUSIONS

The present study leads to the following main conclusions.

(1) Reddening across the observed cluster regions of NGC 3105, NGC 3603, Melotte 105, Hogg 15 and Pismis 20 seems to be non-uniform, with corresponding mean values of $E(B-V) = 1.06$, 1.44, 0.52, 1.50 and 1.55 mag respectively. The law of interstellar extinction in the direction of these and the NGC 4815 and NGC 6253 cluster regions appears normal.

(2) Visual fittings of the ZAMS and/or isochrones to the cluster sequence in the $V_0, (U-B)_0$ $V_0, (B-V)_0$, $V_0, (V-R)_0$ and $V_0, (V-I)_0$ diagrams over a broad range of V magnitude (~5) give distances of 9.5 ± 1.5 kpc to NGC 3105, 7.2 ± 1.2 kpc to NGC 3603, 2.3 ± 0.2 kpc to Melotte 105, 3.8 ± 0.3 kpc to Hogg 15, 2.8 ± 0.2 kpc to NGC 4815, 3.6 ± 0.4 kpc to Pismis 20 and 1.8 ± 0.1 kpc to NGC 6253.

(3) Theoretical isochrones with convective core overshooting fitted to the bright cluster members indicate that the oldest cluster in the sample is NGC 6253 with an age of ~2.5 Gyr, and the youngest one is NGC 3603 with an age of ~3 Myr. Both Hogg 15 and Pismis 20 are of the same age, ~6 Myr. NGC 3105, Melotte 105 and NGC 4815 are all older than 10 Myr with ages ~25, 250 and 400 Myr respectively.

(4) The dynamical evolutionary effects probably have not affected the IMF of the clusters under study (except for NGC 6253), as they are younger than 500 Myr, which is a typical time-scale for dynamics to affect the IMF of the stellar systems. Their present-day MF therefore can be assumed to be equivalent to the IMF. The MF slopes of these clusters agree with the value of the Salpeter MF slope in the solar neighbourhood, considering the scatter produced by Poisson noise (see Kroupa 2001). Also, the MF slopes of young clusters have no dependence on Galactic longitude, R_G and cluster age. All these support the idea of an universal IMF in Galactic star-forming regions above 1 $M_\odot$, as they are located in different parts of our Galaxy. In the oldest cluster of the sample, the MF could be estimated only in a narrow mass range. This MF is quite different from those of young clusters, but similar to those of other older systems, indicating an evaporation of low-mass cluster members as a result of dynamical evolution.

(5) The radial distribution of stellar surface density indicates that (except for NGC 6253) all the clusters under study are compact.

(6) WR stars and blue supergiants are observed only in clusters younger than 10 Myr, while red giants are observed only in those older than about 20 Myr. However, blue stragglers seem to be present in clusters of all ages.

(7) In NGC 4815, star 8692 is a candidate for an interacting binary.

ACKNOWLEDGMENTS

We gratefully acknowledge the valuable comments and suggestions given by the referee J.-C. Mermilliod. The generous telescope time allocation for this project and the financial support to UM provided by the SAAO is gratefully acknowledged. We have used the Open Cluster Data Base maintained by J.-C. Mermilliod in the present work. One of us (RS) acknowledges financial help provided by the Alexander von Humboldt Foundation for staying in Germany and completing this paper.

REFERENCES

Ahumada J., Lapasset E., 1995, A&AS, 109, 375
Ahumada A. V., Claria J. J., Bica E., Piatti A. E., 2000, A&AS, 141, 79
Alcalá J. M., Ferro A. A., 1988, Rev. Mex. Astron. Astrofis., 16, 81
Balona L. A., Laney C. D., 1995, MNRAS, 277, 250
Barbon R., Carraro G., Munari U., Zwitter T., Tomasella L., 2000, A&AS, 144, 451
Bertelli G., Bressan A., Chiosi C., Fagotto F., Nasi E., 1994, A&AS, 106, 275
Bragaglia A., Tessicini G., Tosi M., Marconi G., Munari U., 1997, MNRAS, 284, 477
Carraro G., Ortolani S., 1994, A&AS, 106, 573
Carretta E., Bragaglia A., Tosi M., Marconi G., 2000, in Pallavicini R., Micela G., Sciortino S., eds, ASP Conf. Ser. Vol. 198, Stellar Clusters and Associations. Astron. Soc. Pac., San Francisco, p. 273
Chen B., Carraro G., Torra J., Jordi C., 1998, A&A, 331, 916
Dean J. F., Warren P. R., Cousins A. W. J., 1978, MNRAS, 183, 569
Drissen L., Moffat A. F. J., Walborn N. R., Shara M. M., 1995, AJ, 110, 2235
Eisenhauer F., Quirrenbach A., Zinnecker H., Genzel R., 1998, ApJ, 498, 278
Elmegreen B. G., 2000, ApJ, 539, 342
Feinstein A., Marraco H. G., 1971, PASP, 83, 218
FitzGerald M. P., Jackson P. D., Moffat A. F. J., 1977, A&A, 59, 141
Francic S. P., 1989, AJ, 98, 888
Hofmann K.-H., Seggewiss W., Weigelt G., 1995, A&A, 300, 403
Hogg A. R., 1965, PASP, 77, 440
Johnson H. L., Morgan W. W., 1953, ApJ, 117, 313
Kjeldsen H., Frandsen S., 1991, A&AS, 87, 119
Koornneef J., 1983, A&A, 128, 84
Kroupa P., 2001, MNRAS, 322, 231
Larson R. B., 1999, in Nakamoto T., ed., Star Formation. Nobeyama Radio Observatory, Japan, p. 336
Lauberts A., 1982, The ESO/Uppsala Survey of the ESO (B) Atlas. European Southern Observatory, Garching
Lyngå G., 1968, The Observatory, 88, 20
Lyngå G., 1987, Catalogue of Open Cluster Data. 5th edn. CDS, Strasbourg, 1/1 S7041

Lyngå G., Wramdemark S., 1973, A&AS, 12, 365
Mathis J. S., 1990, ARA&A, 28, 37
Melnick J., Grosbol P., 1982, A&A, 107, 23
Melnick J., Tapia M., Terlevich R., 1989, A&A, 213, 89
Menzies J. W., Cousins A. W. J., Banfield R. M., Laing J. D., 1989, S. Af. Astron. Obs. Circ., 13, 1
Mermilliod J. C., 1995, in Egret E., Abrecht M. A., eds, Information and On-line Data in Astronomy. Kluwer, Dordrecht, p. 227
Moffat A. F. J., 1974a, A&A, 34, 29
Moffat A. F. J., 1974b, A&A, 35, 315
Moffat A. F. J., 1983, A&A, 124, 273
Moffat A. F. J., FitzGerald M. P., 1974, A&AS, 16, 25
Moffat A. F. J., Vogt N., 1973, A&AS, 10, 135
Moffat A. F. J., Drissen L., Shara M. M., 1994, ApJ, 436, 183
Munari U., Carraro G., 1995, MNRAS, 277, 1269
Munari U., Carraro G., 1996, MNRAS, 283, 905
Munari U., Tudin B. F., Taranova O. G., Massone G., Maranz F., Roberts G., Winkler H., Whitelock P. A., 1992, A&AS, 93, 383
Munari U., Carraro G., Barbon R., 1998, MNRAS, 297, 867
Muzzio J. C., 1979, AJ, 84, 639
Muzzio J. C., Feinstein A., Orsatti A. M., 1976, PASP, 88, 526
Pandey A. K., Ogura K., Sekiguchi K., 2000, PASJ, 52, 847
Peterson C. J., FitzGerald M. P., 1988, MNRAS, 235, 1439
Phelps R. L., Janes K. A., 1993, AJ, 106, 1870
Phelps R. L., Janes K. A., Montgomery K. A., 1994, AJ, 107, 1079
Piatti A. E., Claria J. J., Bica E., Geisler D., Minniti D., 1998, AJ, 116, 801
Piskunov A. E., 1976, Nauch. Inf., 22, 47
Richtler T., Sagar R., 2001, Bull. Astron. Soc. India, 29, 53
Sagar R., 1987, MNRAS, 228, 483
Sagar R., 2000, Bull. Astron. Soc. India, 28, 55
Sagar R., Cannon R. D., 1994, Bull. Astron. Soc. India, 22, 381
Sagar R., Griffiths W. K., 1998a, MNRAS, 299, 1
Sagar R., Griffiths W. K., 1998b, MNRAS, 299, 777
Sagar R., Joshi U. C., 1979, Ap&SS, 66, 3
Sagar R., Richtler T., 1991, A&A, 250, 324
Sagar R., Piskunov A. E., Myakutin V. I., Joshi U. C., 1986, MNRAS, 220, 383
Sagar R., Myakutin V. I., Piskunov A. E., Dluzhnevskaya O. B., 1988, MNRAS, 234, 831
Salpeter E. E., 1955, ApJ, 121, 161
Sanner J., Geffert M., 2001, A&A, 370, 87
Santos J. F. C., Jr, Bica E., 1993, MNRAS, 260, 915
Scalo J. M., 1986, Fundam. Cosmic Phys., 11, 1
Scalo J. M., 1998, in Gilmore G., Parry I., Ryan S., eds, ASP Conf. Ser. Vol. 142, The Stellar Initial Mass Function. Astron. Soc. Pac., San Francisco, p. 201
Schaller G., Schaerer D., Meynet G., Maeder A., 1992, A&AS, 96, 269
Schmidt-Kaler Th., 1982, in Scaifers K., Voigt H. H., eds, Landolt/Bornstein, New Series, Group VI, Vol. 2b, Numerical Data and Functional Relationship in Science and Technology. Springer-Verlag, Berlin, p. 14
Sher D., 1965, MNRAS, 129, 237
Stetson P. B., 1987, PASP, 99, 191
Stetson P. B., 1992, in Worrall D. M., Biemesderfer C., Barnes J., eds, ASP Conf. Ser. Vol. 25, Astronomical Data Analysis Software and Systems I. Astron. Soc. Pac., San Francisco, p. 297
Subramaniam A., Sagar R., 1999, AJ, 117, 937
Turner D. G., 1996, AJ, 111, 828
van den Bergh S., 1978, A&A, 63, 275
van den Bergh S., Hagen G. L., 1975, AJ, 80, 11
van den Bergh S., Sher D., 1960, Publ. David Dunlop Obs., 2, 203
Vázquez R. A., Will J.-M., Prado P., Feinstein A., 1995, A&AS, 111, 85
Walker A. R., 1985, MNRAS, 213, 889
Walker A. R., 1987, MNRAS, 229, 31

This paper has been typeset from a TEX/LATEX file prepared by the author.